A Dynamic Transformation Car-Following Model for the Prediction of the Traffic Flow Oscillation



©SHUTTERSTOCK.COM/E2DAN

Shan Fang , Lan Yang , Xiangmo Zhao, Wei Wang , and Zhigang Xu

Are with the School of Information Engineering, Chang'an University, Xi'an 710064, China. E-mail: fang6100146@gmail. com; lanyang@chd.edu.cn; xmzhao@chd.end.cn; wei.wang@chd.edu.cn; xuzhigang@chd.edu.cn

Guoyuan Wu

Is with the Center for Environmental Research and Technology, University of California at Riverside, Riverside, CA 92521-9800 USA. E-mail: guoyuan.wu@ucr.edu

Yang Liu 🔍

Is with the Department of Architecture and Civil Engineering, Chalmers University of Technology, 412 96 Gothenburg, Sweden. E-mail: liuy@chalmers.se

Xiaobo Qu

Is with the State Key Laboratory of Automotive Safety and Energy, School of Vehicle and Mobility, Tsinghua University, Beijing 100084, China. E-mail: xiaobo@tsinghua.edu.cn

Digital Object Identifier 10.1109/MITS.2023.3317081 Date of current version: 20 October 2023

*Corresponding author

Abstract—Car-following (CF) behavior is a fundamental of traffic flow modeling; it can be used for the virtual testing of connected and automated vehicles and the simulation of various types of traffic flow, such as free flow and traffic oscillation. Although existing CF models can replicate the free flow well, they are incapable of simulating complicated traffic oscillation, and it is difficult to strike a balance between accuracy and efficiency. This article investigates the error variation when the traffic oscillation is simulated by the intelligent driver model (IDM). Then, it divides the traffic oscillation into four phases (coasting, deceleration, acceleration, and stationary) by using the space headway of multiple steps. To simulate traffic oscillation between multiple human-driven vehicles, a dynamic transformation CF model is proposed, which includes the long-time prediction submodel [modified sequence-to-sequence (Seq2seq)] model, short-time prediction submodel (Transformer), and their dynamic transformation strategy]. The first submodel is utilized to simulate the coasting and stationary phases, while the second submodel is utilized to simulate the acceleration and deceleration phases. The results of experiments indicated that compared to K-nearest neighbors, IDM, and Seq2seq CF models, the dynamic transformation CF model reduces the trajectory error by 60.79–66.69% in microscopic traffic flow simulations, 7.71–29.91% in mesoscopic traffic flow simulations, and 1.59–18.26% in macroscopic traffic flow simulations. Moreover, the runtime of the dynamic transformation CF model (Inference) decreased by 14.45–66.17% when simulating the large-scale traffic flow.

he car-following (CF) model is an essential component of traffic flow simulation for the human-driven vehicle (HV) and connected and automated vehicle (CAV). Some CF models have been widely used in mixed traffic flow modeling [1], virtual testing of CAV [2], [3], [4], [5], [6], [7], [8], and the trajectory planning of CAV [9], [10], [11], [12], [13], [14].

Introduction

Currently, even though the existing CF models [16], [17] can simulate the free flow well, they suffer from the following two issues. First, existing CF models may not perform well when simulating traffic oscillation, also known as stop-andgo waves [17], [18], [19]. Because traffic oscillation exhibits frequent acceleration and deceleration behavior, existing CF models cannot accurately simulate the change in CF behavior at each time step. In addition, there may be significant errors when using the CF model to replicate traffic capacity, vehicle energy consumption, and the formation and dissipation of stop-and-go waves in the traffic oscillation region. The second issue is that the existing data-driven CF models may necessitate costly computational resources and considerable computation time when generating large-scale traffic flow [20]. They both severely restrict the applicability of the CF models.

To resolve the issues mentioned previously, this article investigates in depth the reasons why the model-driven CF model and data-driven model cannot simulate the traffic oscillation more accurately and uses the space headway of multiple steps to classify the traffic oscillation into four phases: coasting, deceleration, acceleration, and stationery. A novel data-driven dynamic transformation CF model consisting of the long-time prediction submodel based on the modified sequence-to-sequence (Seq2seq) model and the

short-time prediction submodel based on the Transformer [21] is then proposed to achieve a balance between accuracy and efficiency for the simulation of traffic oscillation between multiple HVs. Among them, the long-time prediction submodel is responsible for the coasting and stationary phases simulation, and the short-time prediction submodel is responsible for the acceleration and deceleration phases simulation. To validate the proposed dynamic transformation CF model, CF pairs are extracted from the Next Generation Simulation (NGSIM) dataset to compare the ability of different data-driven CF models to extract the features of CF behavior at past multiple time steps and to comprehensively and objectively evaluate the dynamic transformation CF model and three other representative CF models from micro, meso, and macro perspectives. In addition, the runtime required to generate large-scale traffic flow for each of the CF models is compared.

In summary, the contributions of this article are as follows:

- 1) This article provides an in-depth analysis of the error variation in the IDM simulation of traffic oscillations. By simplifying the expression of the IDM in the deceleration phase, it is shown that the derivative function of the kinematic acceleration is a monotonically decreasing trend, i.e., the simulated vehicle position is greater than the actual position. The error accumulation and inequality property then prove that the trajectory error increases when IDM simulates the vehicle acceleration behavior.
- 2) A transformation strategy that dynamically divides realistic traffic oscillation into four phases, including coasting, deceleration, acceleration, and stationary, is designed. Analyzing the NGSIM dataset, the space headway of multiple steps as the more direct traffic parameter is selected as the phase judgment condition of the traffic oscillation. To the best of our knowledge, no previous studies have

decomposed traffic oscillations into different phases using micro vehicle dynamic parameters.

3) A dynamic transformation CF model consisting of two submodels is proposed. The long-time prediction submodel based on the modified Seq2seq architecture is utilized for the simulation of the coasting or stationary phases, whereas the short-time prediction submodel based on the Transformer model is utilized for the simulation of the acceleration or deceleration phases. Our proposed model is the first model that attempts to simulate traffic oscillation using multiple submodels as opposed to existing models.

The rest of the article is organized as follows. The "Related Work" section briefly reviews two different types of CF models (data-driven and model-driven modeling) and related research on traffic oscillation. The "Problem Description" section describes two issues with existing CF models; the IDM CF model is unable to accurately simulate traffic oscillation, and the deep learning (DL) CF model does not account for the inherent correlation between different vehicle dynamic parameters at the same time step. In the "Methodology" section, the proposed dynamic transformation CF model is introduced in depth, and the dynamic transformation strategy for the two submodels of the dynamic transformation CF model is designed. The dynamic transformation CF model is validated and tested in the

T 111	4 8 8		
Iania	רואו ד	iinr nn	tations.
ιαυισ	I. IVIO	טוו וטןו	tations.

Parameters	Definition
t	Current time step
Δt	Time step of two adjacent data points
T_{ρ}	Time steps of historical data
T_f	Time steps of prediction data
a_{p}	Acceleration of the preceding vehicle
a_{f}	Acceleration of the FV
V_{ρ}	Velocity of the preceding vehicle
V_f	Velocity of the FV
ρ_p	Position of the preceding vehicle
ρ_f	Position of the FV
Δp	Space headway
ΔV	Velocity difference
a_{\max}	Max acceleration of the FV
d_{com}	Comfortable deceleration of the FV
S_0	Space headway at stationary
T	Desired time headway
S_d	Desired space headway
V_d	Desired velocity
a_d	Desired acceleration

"Experiments" section. The "Conclusion" section concludes the article.

Related Work

Before delving into analysis, the notations used are defined as shown in Table 1.

Model-Driven CF Models

The model-driven CF models reveal the mapping relationships between the microscopic parameters of vehicle dynamics with the functional expressions. The well-known model-driven CF models are the full velocity difference CF model, the Newell CF model, and the intelligent driver model (IDM) CF model [22], [23], [24]. They have been used for traffic oscillation analysis because each parameter of the model-driven model has an explicit physical meaning. The Newell CF model was used on traffic oscillation measurements in the frequency domain of the trajectory [25]. Then, with the help of the describing-function approach, it was enhanced to mitigate the traffic oscillation and decrease the fuel consumption of vehicles [26]. Furthermore, the time domain of the trajectory was considered to calibrate the parameters of the Newell CF model [27]. To alleviate the traffic oscillation, the IDM CF model was used as the stability criterion to develop the oscillation criterion to identify different categories of traffic oscillation [28].

Data-Driven CF Models

The data-driven CF model is primarily constructed using machine learning (ML), reinforcement learning (RL), and DL. K-nearest neighbors (KNN), fixed-radius NN (FRNN), and deep deterministic policy gradient (DDPG), three representative ML and RL algorithms, have been widely used in CF behavior modeling [20], [29], [30], [31], [33], [34], [35], [36], [37]. Compared to the CF models based on ML and RL, DL-based CF model research has been used longer and produced more results. Some of the representative data-driven CF models are summarized in Table 2. Literature [38], [39], [40], [41], [42] used the artificial neural network (ANN) to simulate CF behavior. The major differences between them are that the input and output of each model differ due to the different influences considered by the model, such as instantaneous reaction delay [41]. In addition, due to limitations imposed by the development of DL, different models employed distinct optimizers. In the literature [42], for instance, the particle swarm optimization algorithm and backpropagation were used to train the model [38], [39], [40], [41].

As the cutting-edge architecture of the DL model, the recurrent NN (RNN) has been widely implemented in numerous research fields. Due to the internal state (or memory) flow mechanism within the RNN, it processes time-series data more efficiently. Zhou et al. [18] proposed a CF model based on the RNN to simulate traffic oscillation

more precisely. To overcome the gradient vanishing and explosion problem of the vanilla RNN model, the gated recurrent unit (GRU) and long short-term memory (LSTM) were utilized to simulate CF behavior, and asymmetric driving behavior was also considered [43], [44]. However, the RNN cannot process the input-output sequences of unequal length. Therefore, Ma and Qu [19] applied the Seg2seg architecture to predict the multi-time steps of the CF. Considering the inefficiency of the conventional CF model in generating vehicle platoon trajectory generation, Lin et al. [45] built a unidirectional interconnected LSTM CF model to simulate CF behavior. Additionally, Mo et al. [17] proposed a CF model that incorporated model-driven modeling and DL and validated the model's performance under the condition of insufficient training data samples. Several popular DL architectures, such as graph attention networks, generative adversarial networks, and Transformer, are [16], [46], [47] are also used for CF behavior modeling. Specifically, Zhou et al. [48] proposed a data-driven framework that was composed of

a signal processing method and short-time Fourier transformation and can be applied to analyze the disturbance amplification in CF behavior.

The aforementioned CF models can be summarized as follows. On the one hand, traffic oscillation studies based on model-driven models may not always be applicable to complicated environments, and more realistic or flexible CF models should be employed to investigate the traffic oscillation. On the other hand, because the traffic oscillation contains many acceleration and deceleration behaviors, even though the existing data-driven CF models can simulate a more complex environment than the model-driven CF models, the accuracy of simulating the traffic oscillation with them still cannot be guaranteed. It can also be seen from Table 2 that some proposed data-driven methods have not been evaluated on the traffic oscillation. In addition, it is concluded that simulating the whole process of traffic oscillation formation and dissipation with a single CF model is difficult, as indicated by [49] that different CF models should be used to simulate the different states of

Table 2. A summary	of existing data-driven CF models.
Models	Innuts

	Models	Inputs	Outputs	Time Steps	Tested on Traffic Oscillation
ML	KNN [28]	Δp , MD of PV	MD of FV	Single step	Yes
	Gipps + Random Forest [29]	Δp , ΔV , V_f , a_f	V_f	Single step	Yes
	FRNN [30]	Δp , MD of PV	MD of FV	Single step	No
RL	DDPG [31]	Δp , Δv , v_f	a_f	Single step	No
	Improved DDPG [32]	Δp , Δv , v_f	V_f	Single step	No
	DDPG [33]	Δp , ΔV , V_f	a_f	Single step	Yes
	DDPG [34]	Δp , Δv , v_f	a_f	Single step	Yes
	DDPG [35]	Δp , Δv , v_f	a_f	Multistep	No
DL	ANN [36]	Δp , Δv , v_{f} , v_{d}	a_f	Single step	No
	ANN [37]	Δp , V_p	V_f	Single step	Yes
	ANN [38]	Δp , Δv , v_{f} , RD	a_f	Single step	No
	ANN [39]	Δp , Δv , v_f	a_f	Single step	No
	ANN [40]	Δp , ΔV	a_f	Single step	No
	GRU [41]	Δp , ΔV , V_f	V_f	Single step	No
	LSTM [42]	Δp , ΔV , V_f	V_f	Single step	Yes
	Seq2seq [17]	Δp , ΔV , V_f	a_f	Multistep	Yes
	LSTM [43]	State of FV/PV	State of FV	Single step	Yes
	Graph attention network [14]	V_f , a_f , V_p , a_p , S_d , a_d , V_d , Δp	a_f	Single step	No
	IDM + ANN (or LSTM)/OVM + ANN (or LSTM) [14]	Δp , Δv , v_f	a _f	Single step	No
	RNN [16]	MD of PV	MD of FV	Single step	Yes
	Transformer [44]	Δp , ΔV , V_f	V_f	Multistep	No

The last column represents whether the model is tested on the traffic oscillation region. State includes the acceleration, velocity, and trajectory. GRU: gated recurrent unit; LSTM: long short-term memory; MD: moving distance; RD, reaction delay; PV, preceding vehicle; FV, following vehicle; OVM: optimal velocity model.

a realistic traffic oscillation. However, to the best of our knowledge, few studies have considered how to decompose the traffic oscillation and select the appropriate CF model for each stage.

Problem Description

Analysis of IDM Simulated the Traffic Oscillation

Deceleration

The representative model-driven CF model, IDM, which is formulated as the following equation, is used to simulate the CF behavior of the following vehicle (FV):

$$a_f = a_{\text{max}} \left[1 - \left(\frac{v_f}{v_d} \right)^{\delta} - \left(\frac{s_d}{\Delta p} \right)^2 \right] \tag{1}$$

where the s_d is defined as follows:

$$s_d = s_0 + \max\left(0, v_f T + \frac{v_f \Delta v}{2\sqrt{a_{\text{max}} a_{\text{com}}}}\right). \tag{2}$$

Typically, the FV first needs to decelerate and then accelerate when passing through a traffic oscillation. When traffic becomes more congested, the FV may come to a complete stop. The deceleration phase occurs when the velocity of the FV is gradually reduced to zero, and the stationary phase occurs when the velocity of the FV remains at zero. The acceleration phase occurs when the velocity of the FV accelerates to the desired velocity, i.e., accelerates until the preceding vehicle and the FV are relatively stationary. In addition, because the vehicle stopping position is related to the vehicle deceleration phase, the errors in the deceleration and acceleration phases are the focus of this article.

Model-Driven Modeling Methods

When the vehicle is in the deceleration phase, the term $a_{\max}(1-(v_f(t)/v_d)^{\delta})$ describing the free-flow CF behavior in the IDM can be ignored. Then, (1) can be simplified to

$$a_f = a_{\text{max}} \left[1 - \left(\frac{v_f}{v_d} \right)^{\delta} - \left(\frac{s_d}{\Delta p} \right)^2 \right].$$
 (5)

According to the definition of the optimal space headway s_d , there are two functional expressions for acceleration

$$a_{f} = \begin{cases} -a_{\text{max}} \left(\frac{s_{0}}{\Delta p}\right)^{2} \\ -a_{\text{max}} \left(\frac{s_{0} + v_{f}T + \frac{v_{f}\Delta v}{2\sqrt{a_{\text{max}}d_{\text{com}}}}}{\Delta p}\right)^{2}. \end{cases}$$
(4)

For the nonemergency braking deceleration phase, the inequality $v_f T + \left(v_f \Delta v/2 \sqrt{a_{\rm max} d_{\rm com}}\right) > 0$ is constant, and the steady-state term $s_0 + v_f T$ can be ignored [50]. Then, (4) can be further simplified to

$$a_f = -a_{\text{max}} \left(\frac{v_f \Delta v}{2\Delta p \sqrt{a_{\text{max}} d_{\text{com}}}} \right)^2 = -\frac{(v_f)^2 \Delta v^2}{4d_{\text{com}} (\Delta p)^2}.$$
 (5)

When the FV is under traffic disturbance and the preceding vehicle is stationary, $\Delta v = v_f$, and then (5) is transformed into the following equation:

$$a_f = -\frac{a^2}{d_{\text{com}}}. (6)$$

In (6), $a=(v_f)^2/2\Delta p$ is the kinematic deceleration, which indicates that the braking distance is equal to the space headway Δp . For the nonemergency braking deceleration phase, the absolute value of the actual deceleration $|a_f|$ is less than the kinematic deceleration a. Thus, we can get the following inequality: $a^2/d_{\rm com} < a$; simplifying the inequality yields $a < d_{\rm com}$. It indicates that the actual deceleration of the FV simulated by IDM is less than the comfortable deceleration at the beginning of the deceleration phase. Furthermore, the partial derivative of a with respect to t is

$$\frac{da}{dt} = \frac{va}{\Delta p d_{\text{com}}} (d_{\text{com}} - a). \tag{7}$$

Equation (7) and $a < d_{\rm com}$ represent that the derivative function of the kinematic acceleration is a monotonically decreasing trend and indicate that the actual deceleration gradually approaches the comfortable deceleration with time. In contrast, human drivers usually adopt the larger deceleration rather than the comfortable deceleration during the deceleration phase because they cannot accurately assess the risk of collision with the FV.

According to the conclusion obtained from the analysis of the deceleration phase, note that the simulated trajectory of the FV by the IDM CF model is s_1 , and the real trajectory of the FV is s_2 . Then, the following equation holds:

$$s_1 > s_2$$
. (8)

Acceleration

In addition, according to the property that the direction of an inequality does not change when both sides are multiplied by a positive number but changes when multiplied by a negative number, the following holds:

$$-a_{\max} \left(\frac{s_d}{\Delta p_1} \right)^2 < -a_{\max} \left(\frac{s_d}{\Delta p_2} \right)^2 \tag{9}$$

where the Δp_1 is the space headway simulated by the IDM when the preceding vehicle and FV are stationary, and the Δp_2 is the actual space headway when the preceding vehicle

and FV are stationary. Thus, the vehicle position simulated by IDM obtained by numerical integration is lower than the ground-truth data.

Analysis of Existing DL CF Models

The existing DL CF models can be expressed by the following function equation:

$$O = F(I) \tag{10}$$

where the function F is the abstract function expression, and the set I is the input of CF models, which generally consists of several vehicle dynamic parameters, such as acceleration, velocity difference, space headway, etc. O is the output of CF models, usually the velocity or acceleration. I and O can be defined as follows:

$$I = \{(s_1(t-i), ..., s_n(t-i))\}$$
(11)

$$O = \{ (s_1(t+i), ..., s_m(t+i)) \}.$$
 (12)

For the short-time prediction submodel based on the DL, the index parameter i of sets I and O are $\{t-T_p, t-T_p+\Delta t,...,0\}$ and $t+\Delta t$, respectively, which indicates that it takes the historical T_p time-step vehicle dynamic parameters to predict the vehicle dynamic parameter of the FV at the next time step. s is the different vehicle dynamic parameters. n and m are the number of vehicle dynamic parameters. One typical short-time prediction submodel consisting of the two-layer RNN is shown in Figure 1(a), and its formulation is as follows:

$$O(t + \Delta t) = F(I(t, t - \Delta t, \dots, t - T_p)). \tag{13}$$

For the long-time prediction submodel, the index parameters i of sets I and O are $\{t-T_p, t-T_p+\Delta t,...,t\}$ and $\{t+\Delta t, t+2\Delta t,...,t+T_f\}$, respectively, which means that it takes the T_p historical time-step vehicle dynamic parameters to predict the acceleration or velocity of the FV at the T_f time steps. One typical long-time prediction submodel based on the Seq2seq with the RNN as the computing unit is shown in Figure 1(b), and its formulation is as follows:

$$O(t + \Delta t, t + 2\Delta t, ..., t + T_f) = F(I(t, t - \Delta t, ..., t - T_p)).$$
 (14)

It is concluded that the existing DL CF models may not consider the inherent correlation between the output (acceleration) and the inputs (velocity, space headway, and velocity difference) at the same time step.

Methodology

The overall framework diagram of this article is given in Figure 2. Based on the analysis of the two issues mentioned previously, it is necessary to divide the traffic oscillation into

distinct phases and simulate them using distinct CF models. Therefore, the data-driven dynamic transformation CF model is proposed, which consists of two major submodels. The first submodel is the long-time prediction submodel, which is based on the modified Seq2seq architecture and is used to predict the coasting and stationary phases. The long-time prediction submodel is the multistep prediction model. The second submodel is the short-time prediction submodel, which is derived from the Transformer model and is used to predict the acceleration and deceleration phases. The short-time prediction submodel is the single-step prediction model.

In terms of input and output selection for the model, Table 2 reveals that most studies used velocity, space headway, and velocity difference as model inputs and acceleration as the model output. Consequently, the inputs and outputs of the long-time prediction submodel in the dynamic transformation CF model proposed in this article are the same as in most studies. In addition, the inputs of the short-time prediction submodel include the acceleration of the FV for the reasons explained in the following sections.

A Dynamic Transformation Strategy for the Traffic Oscillation Simulation

According to [51], the division of four phases of traffic oscillation depends on the asymmetric traffic theory. However, it remains unclear how micro vehicle dynamic parameters

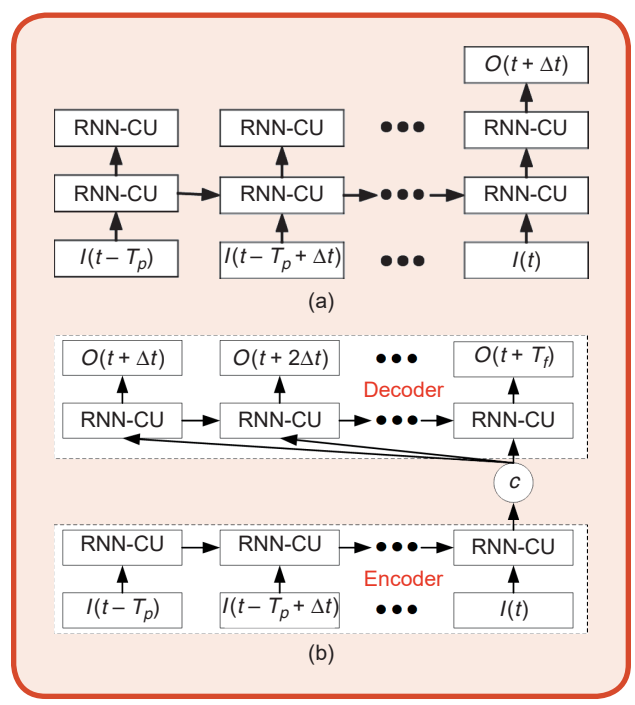


FIG 1 An illustration of the short/long-time prediction CF model. (a) The short-time prediction CF model (b) The long-time prediction CF model. RNN-CU: recurrent neural network-computation unit.

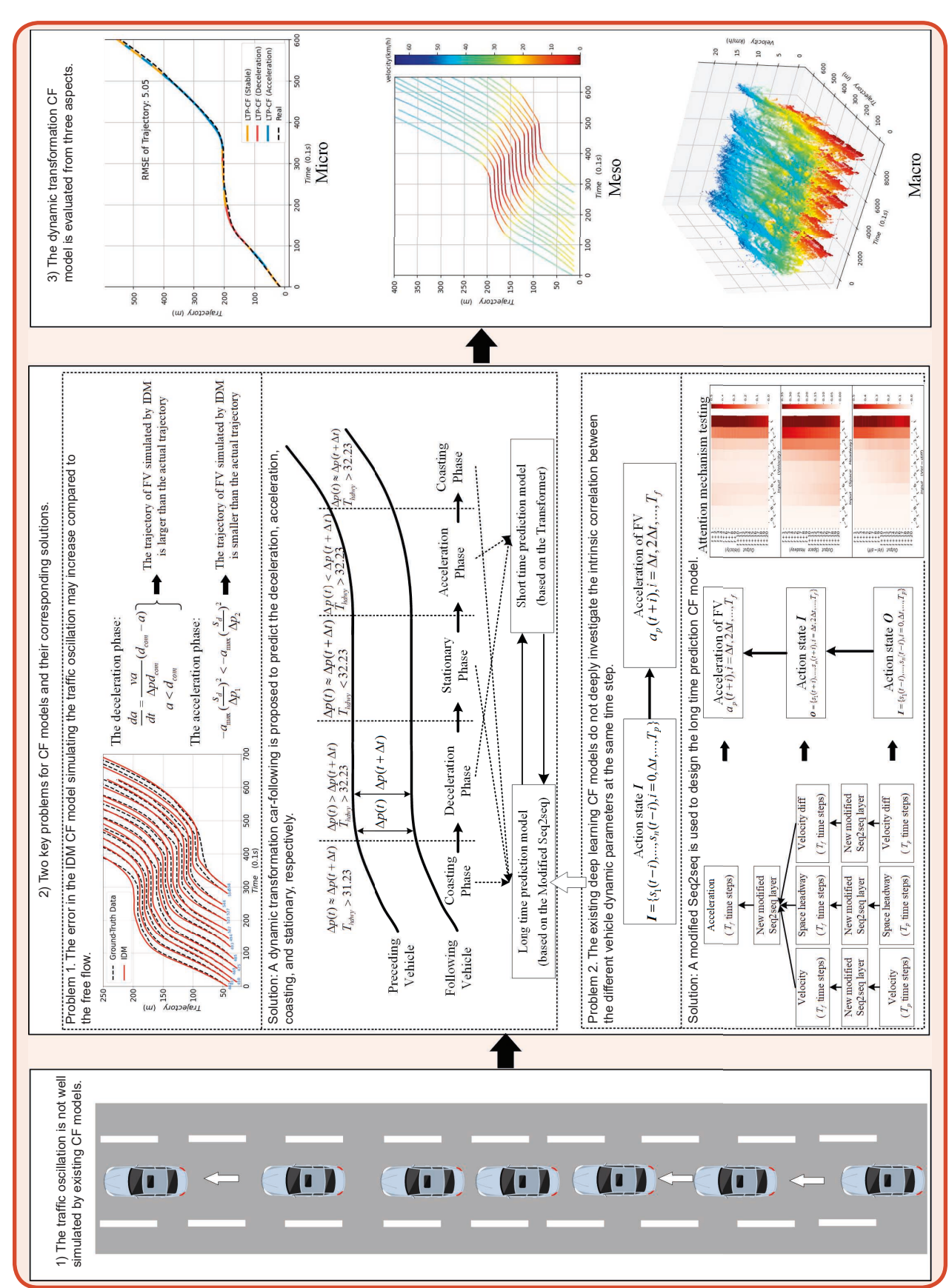


FIG 2 The overall framework of this article. LTP-CF: long time prediction car-following model.

can be used for four-phase identification. The space headway of multi-time steps ($T_{\rm hdwy}$) is used to try to distinguish four phases of the traffic oscillation because it is more stable in a time segment than velocity difference and acceleration. As shown in Figure 3, by analyzing the distribution of the space headway at the stationary phase in the NGSIM dataset, the approximately normal distribution function of the space headway of the stationary phase is $X \sim N(24.72, 627.0016)$. As a determination condition for the stationary state in the traffic oscillation, the 90% probability value of the approximately normal distribution is calculated, i.e., 31.23 ft, to improve the generalization capability of the model.

Figure 4 is a schematic diagram illustrating the traffic oscillation in relation to the $T_{\rm hdwy}$. The distinction between the stationary state and the other states is based on whether the space headway at each time step in $T_{\rm hdwy}$ is fewer than 31.23 ft. The vehicle is in the deceleration phase when the space headway at each time step in $T_{\rm hdwy}$ is greater than 31.25 ft and $T_{\rm hdwy}$ is monotonically decreasing. The vehicle is in the acceleration phase when the space headway at each time step in $T_{\rm hdwy}$ is greater than 31.23 ft and $T_{\rm hdwy}$ is monotonically increasing. A vehicle is determined to be in a stable state if the space headway at each time in $T_{\rm hdwy}$ is greater than 31.23 ft and there is no monotonicity in $T_{\rm hdwy}$.

The dynamic transformation mechanism is described in Algorithm 1 with reference to the definitions of the four phases of traffic oscillation.

The Long-Time Prediction Submodel Based on the Modified Seq2seq

In this section, a novel framework based on the conventional Seq2seq is designed, and then the conventional Seq2seq is improved to obtain the long-time prediction submodel in the dynamic transformation CF model.

Novel Long-Time Prediction Submodel Framework

As illustrated in Figure 5, the proposed long-time prediction submodel framework comprises two modules, with the computation layer (CL) being the conventional Seq2seq.

The first module predicts the velocity, space headway, and velocity difference at T_f time steps using the velocity, space headway, and velocity difference at T_p time steps, respectively. It can be formulated as follows:

$$O(v_f(t + \Delta t), ..., v_f(t + T_f)) = F(I(v_f(t), ..., v_f(t - T_p)))$$
(15)

$$O(\Delta p(t + \Delta t), ..., \Delta p(t + T_f)) = F(I(\Delta p(t), ..., \Delta p(t - T_p)))$$
(16)

$$O(\Delta v(t+\Delta t),...,\Delta v(t+T_f)) = F(I(\Delta v(t),...,\Delta v(t-T_p))).$$
(17)

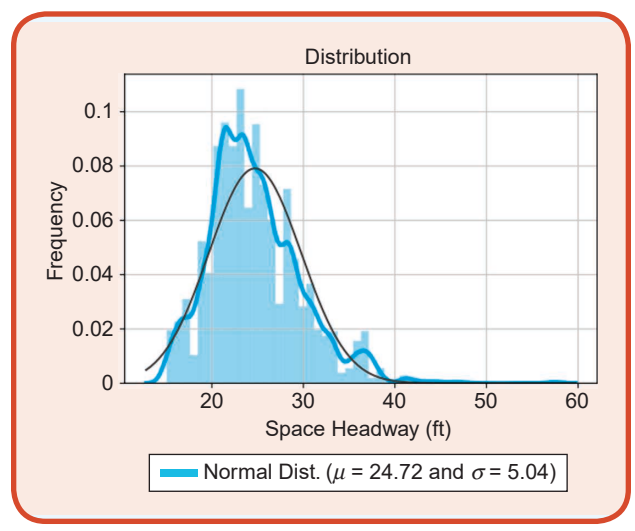


FIG 3 The approximately normal distribution of the space headway at the stationary phase. Normal Dist.: normal distribution.

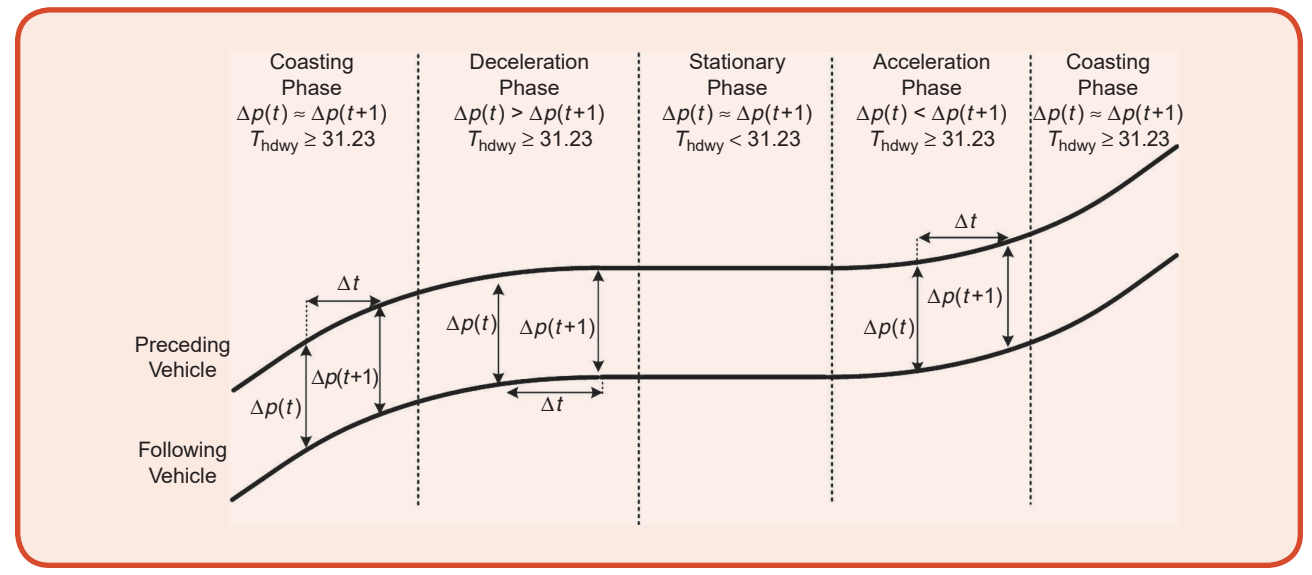


FIG 4 The schematic diagram of the traffic oscillation division according to the T_{hdwv}

The second module predicts the acceleration at T_f time steps with the velocity, space headway, and velocity difference at T_f time steps obtained from the prediction of the first module. It can be formulated as follows:

Algorithm 1: The dynamic transformation strategy.

Input: Velocity of the FV v_l , space headway Δp , velocity difference Δv , total time steps of the trajectory of the preceding vehicle L_{pv}

Output: Acceleration of the FV a_t velocity of the FV v_t , the position of the preceding vehicle p_t

i is the current time step, which is initially set to 0.

```
for i < L_{pv}:
```

Picking the history of 20 time steps of Δp that is denoted as T_{hdwy} from the current time step t

if (
$$T_{hdwy} \ge 31.23$$
) and ($T_{hdwy} \nearrow$)

$$a_f(t + \Delta t) = STP(v_f, \Delta p, \Delta v)$$

else if (
$$T_{hdwy} \ge 31.23$$
) and ($T_{hdwy} \setminus$)

$$a_f(t + \Delta t) = STP(v_f, \Delta p, \Delta v)$$

else if ($T_{hdwy} \ge 31.23$) and T_{hdwy} has no monotonicity

$$a_f(t + \Delta t) = \text{LTP}(v_f, \Delta p, \Delta v)$$

else if (
$$T_{hdwy}$$
 $<$ 31.23)

$$a_f(t + \Delta t) = \text{LTP}(v_f, \Delta p, \Delta v)$$

end if

Update v_f and p_f with a_f

end for

$$O(a_f(t+\Delta t),...,a_f(t+T_f)) = F(O(v_f(t+\Delta t),...,a_f(t+T_f)),$$

$$O(\Delta p(t+\Delta t),...,\Delta p(t+T_f)),$$

$$O(\Delta v(t+\Delta t),...,\Delta v(t+T_f))).$$
(18)

The most critical issue in the proposed long-time prediction submodel framework is how to construct a CL as a CL can be constructed from various DL modules, such as the backpropagation NN (BP-NN), RNN, and Seq2seq. Five representative DL models [BP-NN, RNN, LSTM, Seq2seq, and Seq2seq with attention mechanism (Seq2seq-Att)] are used as the CL to build the long-time prediction submodel to objectively evaluate their performance. The NGSIM dataset, US101, lane 2 subset (the ID of the preceding vehicle is 1989, and the ID of the FV is 2035) is extracted for testing. In addition, the input data length and output data length are both set as 10. The CF data preprocessing and noise filtering processes can be seen in [52].

The min-max normalization that is expressed as follows is used to speed up model convergence:

$$x' = \frac{x - x_{\min}}{x_{\max} - x_{\min}} \tag{19}$$

where x represents the ground-truth data, x' denotes the normalized data, and the x_{\min} and x_{\max} are the min value and max value of x, respectively. In addition, the root mean

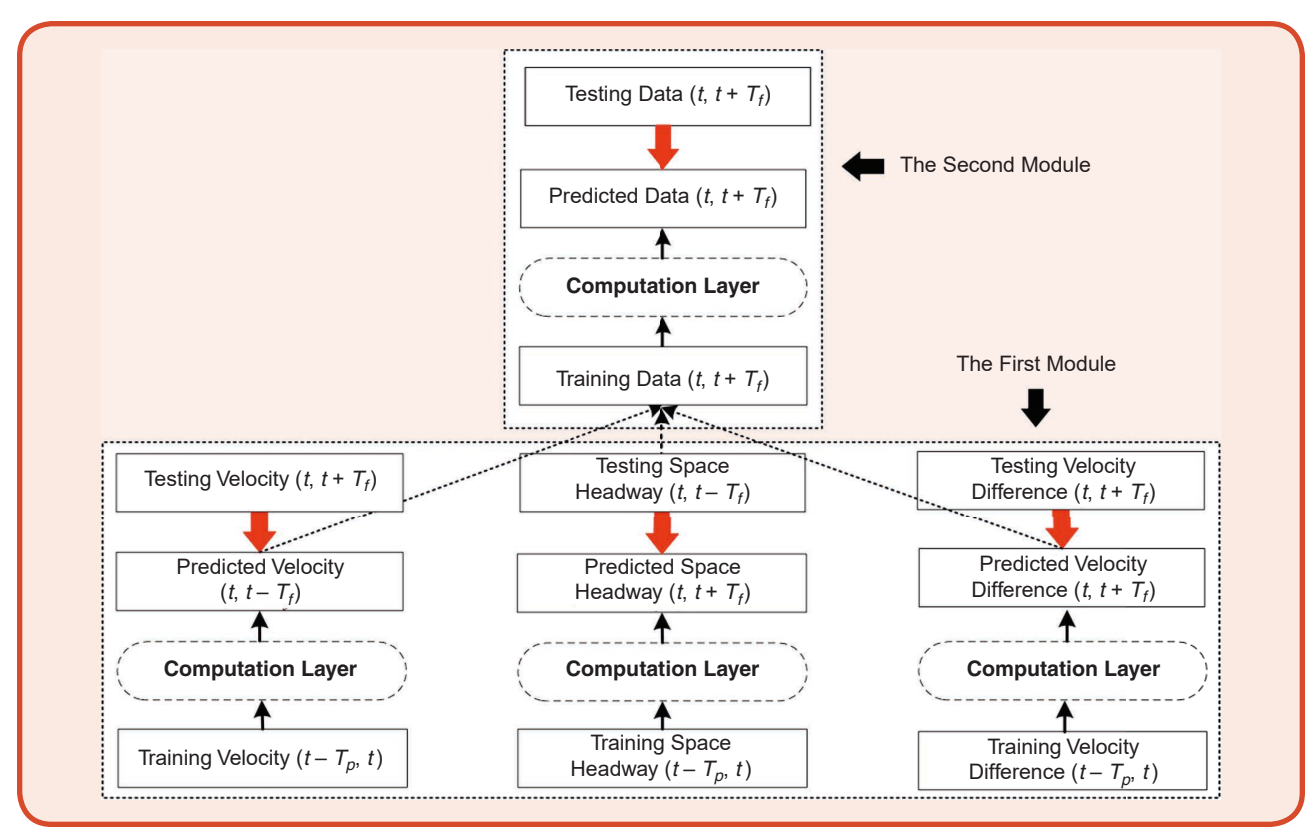


FIG 5 The framework of the long-time prediction submodel.

square error of trajectory (RMSET) is selected to compare the performance of the different CLs. The formulation of the MSET is as follows:

RMSET =
$$\sqrt{\frac{1}{N} \sum_{i=1}^{N} (y_i - \hat{y}_i)^2}$$
 (20)

where N represents the number of samples, and \hat{y}_i and \hat{y}_i are the ith ground-truth trajectory, and prediction trajectory, respectively.

MSET and time-space diagrams for different models or CLs are given in Table 3 and Figure 6, respectively. The trajectories of BP-NN CF and RNN CF are not provided due to their excessive MSET and distorted simulated trajectories. Compared to other data-driven CF models, the long-time prediction submodel framework performed better. Specifically, the MSET of the long-time prediction submodel, which is based on the BP, outperformed the Seq2seq CF model and yielded results similar to the Seq2seq-Att CF model. It demonstrated the performance of the long-time prediction submodel.

On the other hand, Figure 6(a) demonstrates that even the long-time prediction submodel, which is based on the Seq2seq-Att, is incapable of simulating the trajectory accurately when the stop-and-go wave emerged, and the MSET is still relatively high. Here are two explanations.

- The conventional attention mechanism (i.e., the dot product) does not consider the inherent correlation between the vehicle dynamic parameters at the same time steps.
- 2) The conventional Seq2seq simply repeats the hidden state as the Decoder's inputs, so the Decoder receives the same input at each time step.

A New CL Based on the Seq2seq-Att

Figure 7 shows a new CL designed for the long-time prediction submodel. The proposed CL utilizes the 1D convolutional operation to extract the coupled temporal features of the Encoder's and the Decoder's hidden state, and the LSTM is used as the computation unit. Then, instead of the dot-product attention mechanism, bilinear transformation-based attention is used [15]. It can be described as follows:

$$X = \text{Conv1}d(e_{\text{out}}) \tag{21}$$

$$Y = \text{Conv1}d(d_{\text{out}}) \tag{22}$$

$$W = \operatorname{softmax}(X^T W_1 Y) \tag{23}$$

$$attention_{out} = tanh(concat(Y, W)W_2) + b_1$$
 (24)

where e_{out} and d_{out} are the output of the Encoder and Decoder. The W_1 and W_2 are the parameter matrix.

In addition, the proposed CL employs a "step-by-step" methodology as opposed to simply repeating the hidden state. This means that the first input of the Decoder is the same as the last output of the Encoder, and the remaining inputs are the outputs of the computation unit from the previous time step.

The Short-Time Prediction Submodel Based on the Transformer

Compared to the coasting and stationary states, the acceleration changes during the deceleration and acceleration phases are more drastic. If only the long-time prediction submodel is utilized, it may result in significant errors. Therefore, one of the most advanced frameworks, Transformer, is used to predict the acceleration and deceleration of the FV in a single time step.

The Transformer model, like the Seq2seq model, consists of two components: the Encoder and the Decoder.

Table 3. An MSET comparison of the different CL/model.							
Name of CL/ Model	Structure of LTP: (Number of Neurons)	RMSET of Model (m)	RMSET of CL (m)				
BP-NN	3-8-8-1	Nan	31.91				
RNN	32-8-1	408.82	14.84				
LSTM	32-8-1	92.53	14.39				
Seq2seq	32-10-1	47.58	11.61				
Seq2seq-Att	32-10-10-1	28.36	10.9				

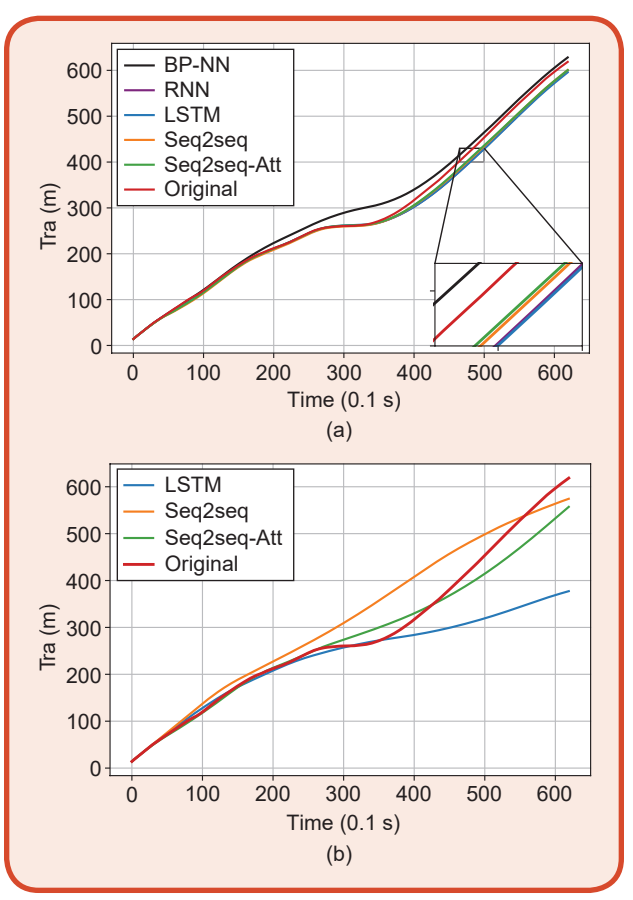


FIG 6 A time-space diagram comparison of different CLs/models.
(a) A time-space diagram of different CLs. (b) A time-space diagram of different models. Tra: trajectory.

When processing time-series data, the Transformer model does not store the temporal information of each time step's data. It requires position encoding to encode the input data of the Encoder and Decoder. The architecture of the Transformer is shown in Figure 8. The Encoder can be seen to consist of three layers: the input layer, the position encoding layer, and the Encoder layer. The Encoder layer is the core of the Encoder, and it is built of a multihead attention block and a residual block. Multihead attention focus improves the Transformer model's ability to handle multidimensional data, while residual blocks increase the model's depth. The Encoder and the Decoder are fundamentally similar in construction, with two exceptions. The first distinction is that the query and value of multihead attention in the Decoder are derived from the semantic vector output by the Encoder. The fully connected (FC) layers are added after the Decoder layer in the Decoder, which is the second distinction. The core part of the Transformer can be formulated as follows:

$$Q = W_q x, K = W_k x, V = W_v x \tag{25}$$

$$A = \operatorname{softmax} \left(\frac{QK^T}{\sqrt{k}} \right) V \tag{26}$$

$$L_{\text{out1}} = \text{LayerNorm}(x + \text{ReLU}(Ax + b1)W_1 + b_2)$$
 (27)

$$L_{\text{out2}} = \text{LayerNorm} \left(L_{\text{out1}} + \text{ReLU} \left(L_{\text{out1}} W_2 \right) \right) \tag{28}$$

where x represents the output of the position layer. W_q , W_k , and W_v are the number of columns of the weight of the K value, and ReLU is the rectified linear unit.

Furthermore, as with [46], the inputs of the Encoder are the acceleration, space headway, and velocity difference of the FV over the previous 10 time steps, and the inputs of the Decoder are the velocity of the preceding vehicle over the

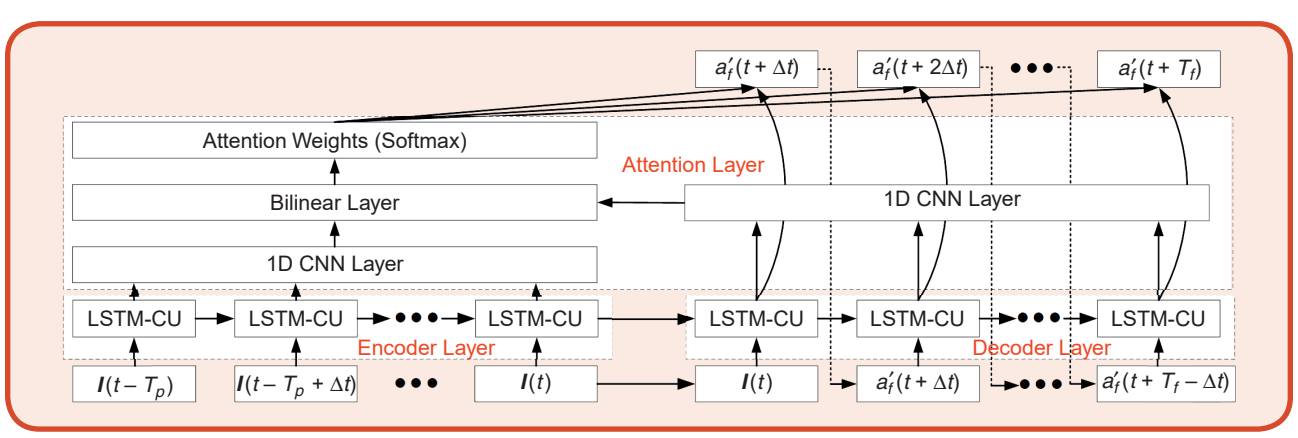


FIG 7 A new CL based on the Seq2Seq-Att.

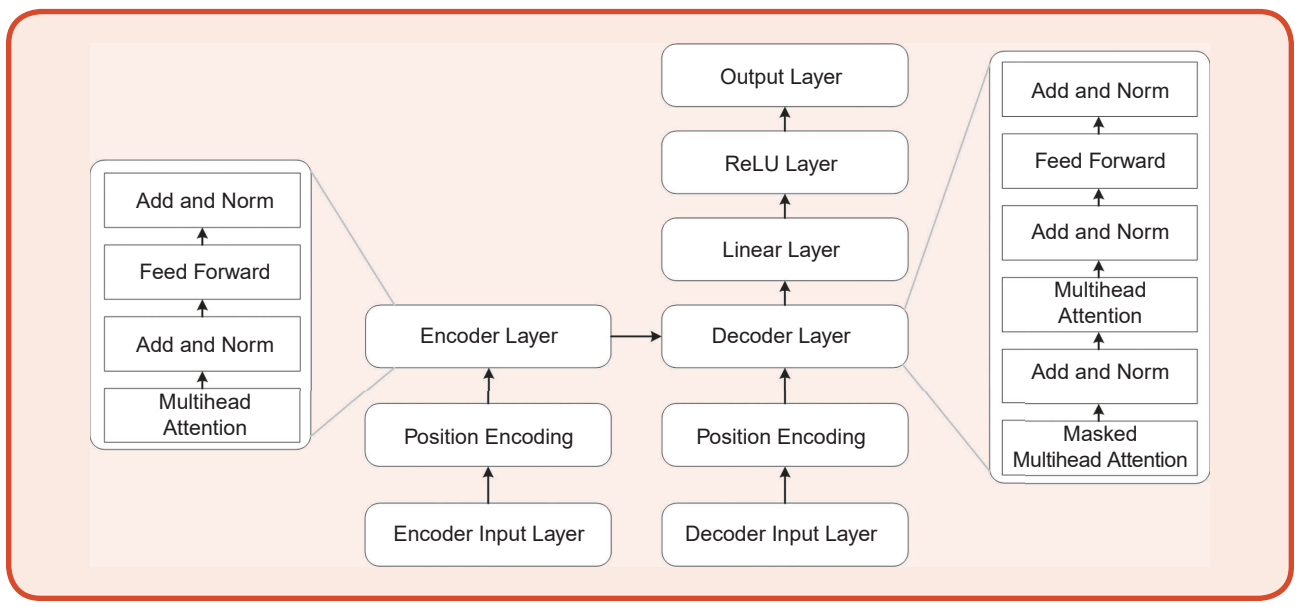


FIG 8 The architecture of the Transformer. ReLU: rectified linear unit.

previous 10 time steps. Therefore, the output of the Decoder of our model is the acceleration of the FV over the subsequent time step.

Experiments

To comprehensively and objectively evaluate the performance of the dynamic transformation CF model, the experimental system framework depicted in Figure 9 is developed in this article. The framework consists of two major components: DL model testing and traffic flow simulation. The "DL Model Test" section conducts hypermeter tuning for the long-time prediction submodel and short-time prediction submodel and chooses the optimal input-output length for the long-time prediction submodel and short-time prediction submodel. Referring to the classification of traffic flow studies by Li et al. [32], the results of four different CF models (dynamic transformation CF model, KNN, IDM, and Seq2seq) are tested for a single CF pair (microscopic level), multiple CF pairs (mesoscopic level), and all CF pairs in one lane within 15 minutes (macroscopic level), and various traffic metrics are used to evaluate the four CF models. In addition, the runtime for generating large-scale traffic flows using four CF models is compared.

DL Model Test

The model is calibrated using the 1,528 CF pairs extracted from the NGSIM dataset in the subset of lane 1 at 8:05 a.m. In the training process, 80% of the data are used for training and 20% for validation. In addition, prior to training, all data are normalized. The entire simulation experiment ran on an

ASUS computer (RAM: 24 GB; processor: Intel Core I7-8700K; operating frequency: 5.70 GHz). Pytorch 1.10 on Windows 10 is deployed to build and test the proposed model.

The Hyperparameter Tuning of the Dynamic Transformation CF Model and the Optimal Input-Output Length for the Long-Time Prediction Submodel

Due to the variable length of the Seq2seq model's input and output variables, the candidate input and output lengths established in this study with reference to the parameter settings of other articles are as follows: input time steps (T=10,20,30,40) and output time steps (T=20,30,40,50). The input time step is observed to be shorter than the output time step. For example, if the input time step is 30, the output time step may be 40 or 50. Therefore, 10 different input-output time-step pairs are tested. Adam is selected as the optimization algorithm to control the gradient descent rule during the calibration process.

The predefined default settings for parameters in Pytorch are adopted (learning rate = 1e-3, $\beta_1=0.9$, $\beta_1=0.999$, epsilon = 1e-8, decay = 0). The activation of an FC layer is a ReLU for the Encoder and Decoder. The performance of the Seq2seq model is affected by two factors: the number of neurons in the LSTM unit and model depth. Since these two influencing factors are coupled, it is challenging to determine the theoretically optimal combination of model parameters. Therefore, the optimal values for parameters other than the model depth and optimal input-output length are obtained using the one-layer stacked long-time prediction submodel. Then, the two-layer stacked long-time prediction submodel,

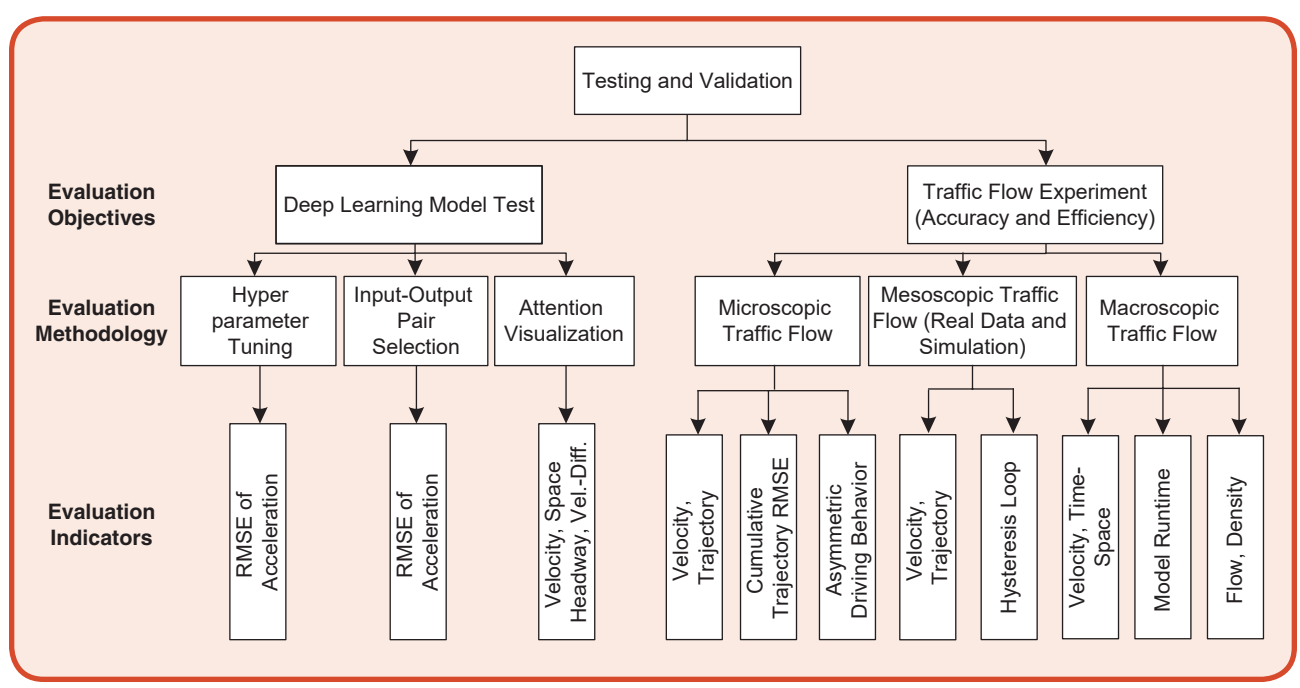


FIG 9 The evaluation framework of the dynamic transformation CF model. Vel.-Diff.: velocity difference.

three-layer stacked long-time prediction submodel, and bidirectional long-time prediction submodel are tested. Table 4 contains the results of parameter tuning.

Table 5 provides the results for a long-time prediction submodel with different layers stacked and different input and output lengths. From Table 5, the following conclusions can be drawn:

1) The mean values of MSE for the one-layer stacked/ two-layer stacked/three-layer stacked/bidirectional long-time prediction submodels are 0.02323, 0.02118, 0.02081, and 0.02131, respectively. This indicates that the MSE of the model further decreases with the increase of the number of model layers, and the more layers, the lower the model MSE. However, the mean MSE at convergence (MSETC) of the three-layer stacked long-time prediction submodel was 1.7% lower than that of the two-layer stacked long-time prediction submodel, whereas the mean one-epoch training time (OETT) increased by 54.8%. Therefore, considering both the algorithm and the accuracy and computation efficiency, a two-layer stacked long-time prediction submodel is chosen as the optimal structure.

Table 4	The parameter settings of the long-time	e
predicti	n submodel	

Parameters	Value
~~~~~~~~~~~~~~~~~~~~~~~~~~~~~~~~~~~~~~~	~~~~~~
The number of neurons in each LSTM unit	32
Hidden neurons of the FC layer (two FC layers)	32.8
Data batch	512
Loss function	MSE

One Cteeled Laver

1.29

4.016

43

29.9

40-50

0.0263

0.02323

Table 5. The performance of the results for the different length input and output.

2) For each layer-stacked architecture, the MSE of the model increased gradually as the length of the input-output pair increased gradually. This is reasonable because a longer output length requires that the model predicts the longtime variation in acceleration. The optimal structure for long-time prediction is 10-20 input-output pairs in which the last 1 s of velocity, space headway, and velocity difference is used to predict the next 2 s of acceleration based on the aforementioned experimental results.

Two key parameters of the short-time prediction submodel based on the Transformer need to be calibrated in comparison to the long-time prediction submodel: the number of the Encoder and Decoder layers and the number of attention heads for multihead attention, respectively. For the shorttime prediction submodel, the input of the model is the last 10 time steps, and the output of the model is the next time step. In addition, the remaining parameters are identical to those of the long-term prediction model.

The results of the short-time prediction submodel of various layers and the number of attention heads are presented in Table 6. These results indicate that the optimal number of attention heads and layers for the short-time prediction submodel is six and four, respectively.

The Seq2seq-Att model (dot product) is chosen for comparison with the long-time prediction submodel to assess the ability of different models to capture the interaction between multiple time steps of the same vehicle dynamic parameter. Figures 10 and 11 depict a visualization result of the attention weights for the long-time prediction submodel and the Seq2seq-Att when predicting velocity, space headway, and velocity difference. The darker red color of the smaller squares indicates that the vehicle dynamics parameters between the two time

Didirectional

1.74

5.464

49

27.5

Three Cteeled Lavers

2.85

10.09

20

22.8

0.0314

0.02131

	Une	Stacked Lay	er	IWO S	Stacked Laye	ers	Inree	Stacked Lay	/ers	BI	Idirectional	~~~~
DTPI (0.1 s)	MSETC	OETT	CE	MSETC	OETT	CE	MSETC	0ETT	CE	MSETC	0ETT	CE
10–20	0.0166	3.7	20	0.0164	5.25	23	0.0162	6.76	27	0.0163	4.87	23
10-30	0.0182	3.93	29	0.0179	5.82	14	0.018	9.93	35	0.0182	5.29	17
10-40	0.0218	4.31	25	0.0209	6.57	22	0.0215	11.77	14	0.0213	5.87	17
10-50	0.0226	4.35	28	0.0233	9.30	29	0.0213	11.99	27	0.0229	6.12	22
20-30	0.0199	4.21	24	0.0194	8.65	29	0.0211	11.05	11	0.0183	5.52	19
20-40	0.0386	4.11	24	0.0203	6.54	33	0.0204	11.43	35	0.0194	6.12	23
20-50	0.0235	5.01	31	0.0226	7.02	24	0.0213	12.26	19	0.0228	6.4	23
30-40	0.0214	4.7	40	0.021	6.75	29	0.0206	11.87	20	0.0202	6.13	28
30-50	0.0234	4.55	35	0.0234	7.18	26	0.0221	10.99	20	0.0223	6.58	54

0.02118 DTPI: different time-step pairs of input-output; MSETC: MSE at Convergence; OETT: one epoch training time (unit: seconds); CE: convergence epoch

0.0266

2.08

6.516

22

25.1

0.0256

0.02081

steps corresponding to the small square are more closely linked. It can be seen that both the Seq2seq-Att model and the long-time prediction submodel are able to describe the correlation of the same vehicle dynamic parameter at multiple time steps. However, the Seq2seq-Att model pays attention to the few recent historical inputs, whereas the long-time prediction submodel can pay attention to many more historical inputs. Figure 11(b) demonstrates, using the space headway as an example, that the future space headway was influenced by the past eight time steps' space headway and that the influence gradually increases with time. In contrast, the Seq2seq-Att model identified only the effect of the past space headway on the future space headway for the three most recent time steps.

### The Comparison of Different Levels of Traffic Flow

In this study, typical micro, meso, and macro traffic flow evaluation indicators are selected to evaluate the performance of the proposed dynamic transformation CF model.

### Microscopic Traffic Flow Simulation

Two CF pairs (the IDs of the FVs are 442 and 1989) are extracted from the dataset to evaluate the performance of the dynamic transformation CF model. Figure 12 illustrates the trajectories generated by the dynamic transformation CF model for vehicles 442 and 1989. It can be seen that the trajectory of the FV is composed of the segmented trajectory generated by the long-time prediction submodel and short-time prediction submodel. When the FV state satisfies the stability condition, the dynamic transformation CF model

Table 6. The results of the different layers and the number of attention heads for the short-time prediction submodel.

Number of Attention Heads	Two Layers	Four Layers	Six Layers
~~~~~	~~~~	~~~~	~~~~
2	0.0059	0.0063	0.0052
4	0.0049	0.0048	0.0048
6	0.0067	0.0046	0.0057

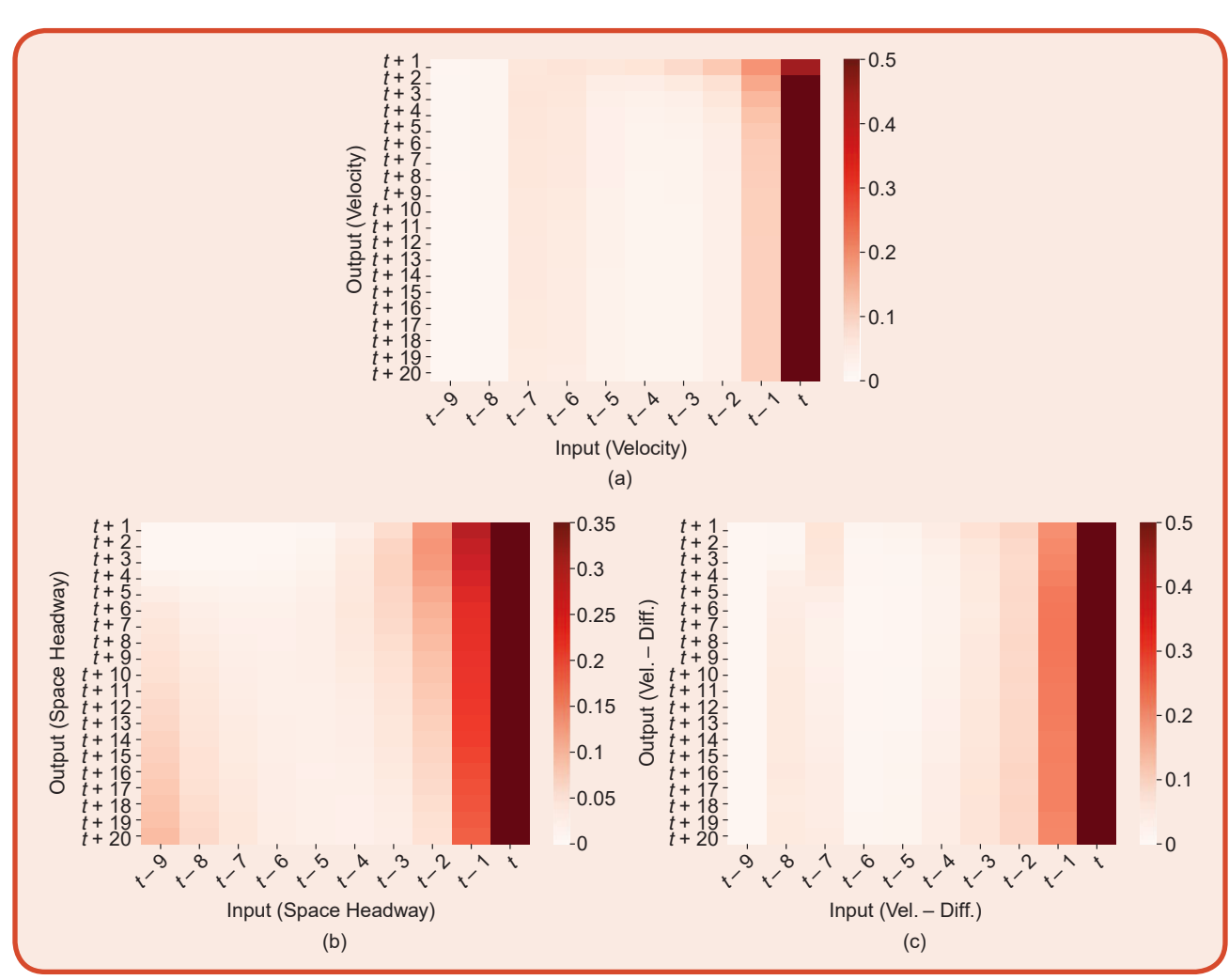


FIG 10 (a)–(c) The attention weights visualization of the Seg2seg with the attention model.

uses the long-time prediction submodel to simulate the trajectory of the FV; when the FV state satisfies the acceleration or deceleration judgment condition, the dynamic transformation CF model uses the short-time prediction submodel model to simulate the trajectory of the FV.

Due to the complexity of the actual traffic flow, it should be noted that the traffic oscillation is not strictly divided into four phases. However, we can use the dynamic transformation strategy to switch between the different phases flexibly. In addition, the RMSEs of the trajectory simulated by the dynamic transformation CF model are 4.78 m and 3.96 m, respectively, indicating that the dynamic transformation CF model can simulate CF behavior with great accuracy.

To comprehensively evaluate the performance of the dynamic transformation CF model, the ground-truth data of vehicle 1989 are used as the test benchmark, and several performance evaluation indexes, such as velocity and space headway, are chosen to test multiple models. Figure 13 (a) and (b) shows the velocity and velocity difference comparison of vehicle 1989. The RMSE of the velocity of IDM is

1.60 m/s, the RMSE of the velocity of KNN is 2.07 m/s, the RMSE of the velocity of Seq2seq is 2.08 m/s, and the RMSE of the velocity of dynamic transformation CF is 1.18 m/s. The results indicated that the dynamic transformation CF model has a lower RMSE and better fitting performance compared to the other three models. In addition, all models are able to simulate the velocity of the FV accurately for the first 30 s, but all models become unstable in the second 30 s. Only the dynamic transformation CF model can consistently and accurately simulate the velocity of the FV.

It can also be seen from Figure 13(a) that the Seq2seq model showed a negative velocity. It is abnormal that the Seq2seq model shows a negative velocity. The reason is that the Seq2seq model is a long-time prediction model, and the model outputs the acceleration for 10 time steps per run. Therefore, the accuracy of the Seq2seq model in simulating CF behavior when the vehicle is in the region of traffic oscillations cannot be guaranteed. This also proves that the Seq2seq model is deficient and needs to be improved. On the contrary, the dynamic transformation CF model outputs

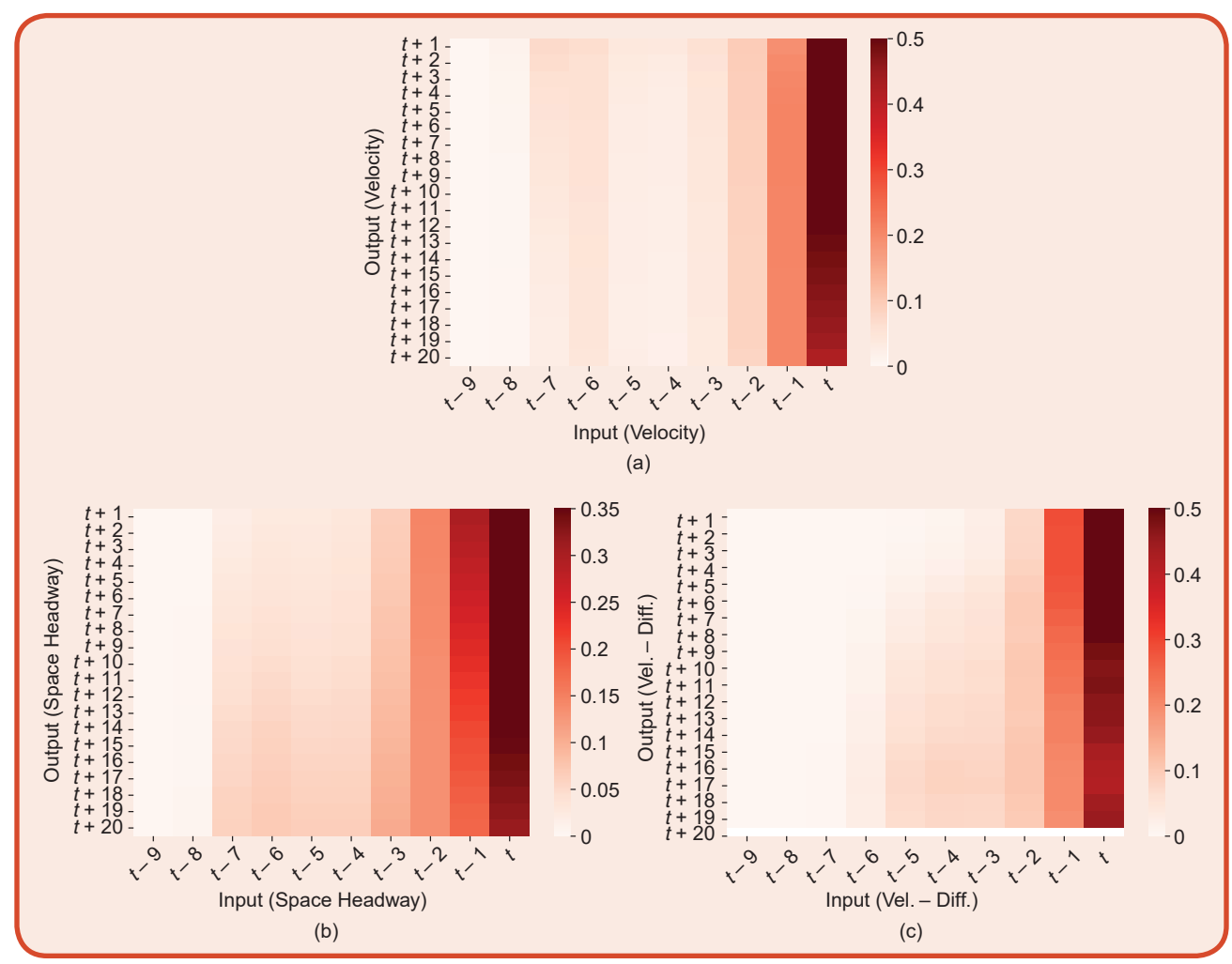


FIG 11 (a)–(c) The attention weights visualization of the long-time prediction submodel.

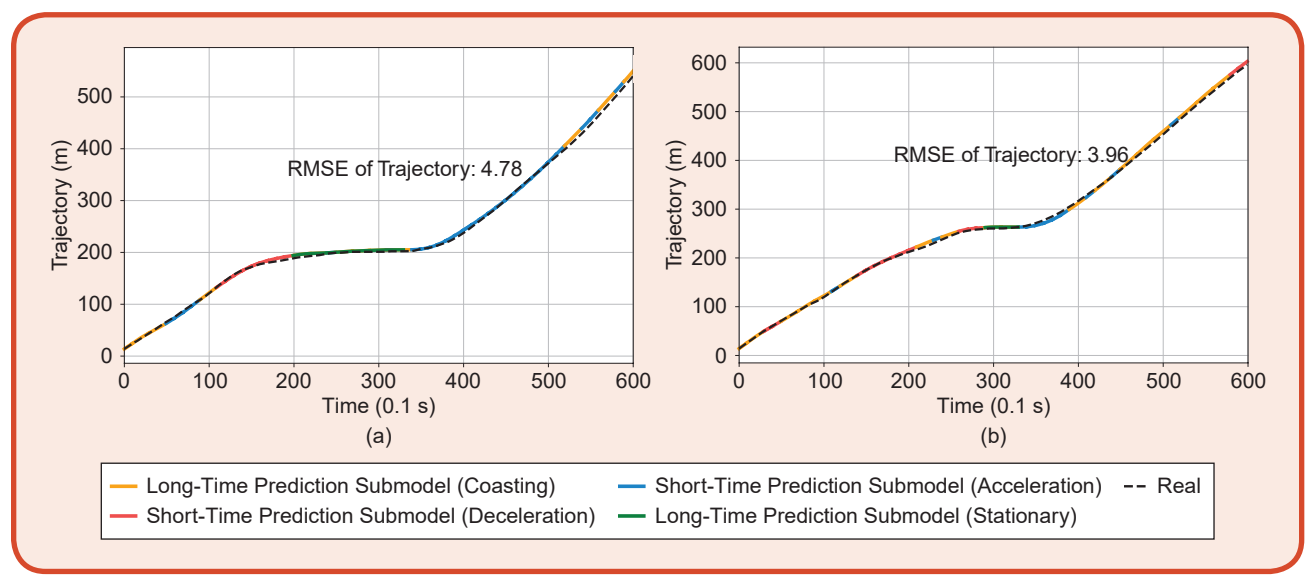


FIG 12 The trajectories of vehicles 442 and 1989 generated by the dynamic transformation CF model. (a) Vehicle 442. (b) Vehicle 1989.

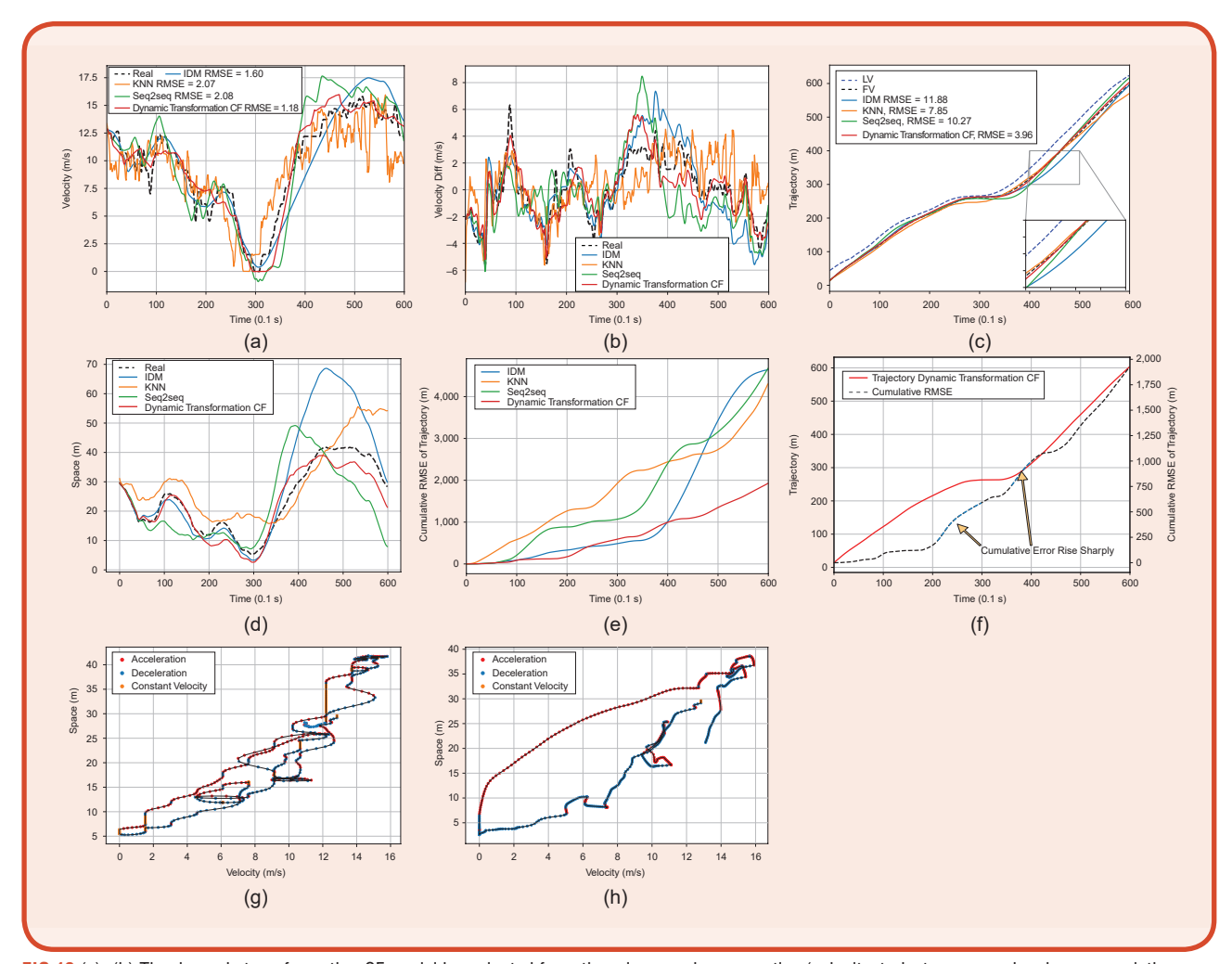


FIG 13 (a)—(h) The dynamic transformation CF model is evaluated from the microscopic perspective (velocity, trajectory, space headway, cumulative trajectory RMSE, and asymmetric driving behavior).

only the acceleration for one time step per run in simulating CF behavior when it is in the region of traffic oscillations, which can increase the accuracy in simulating CF behavior.

Figure 15 (c) and (d) compares the trajectory and space headway of vehicle 1989. Figure 15(c) demonstrates that while all models are able to simulate the trajectory of the FV, the IDM and Seq2seq CF models are unable to accurately simulate the vehicle's reacceleration when it encounters traffic oscillation. Compared to KNN, IDM, and Seq2seq, the dynamic transformation CF model reduces the trajectory error by 60.79–66.95%. Figure 13(d) also reveals that the space headway errors of the IDM and Seq2seq CF models were

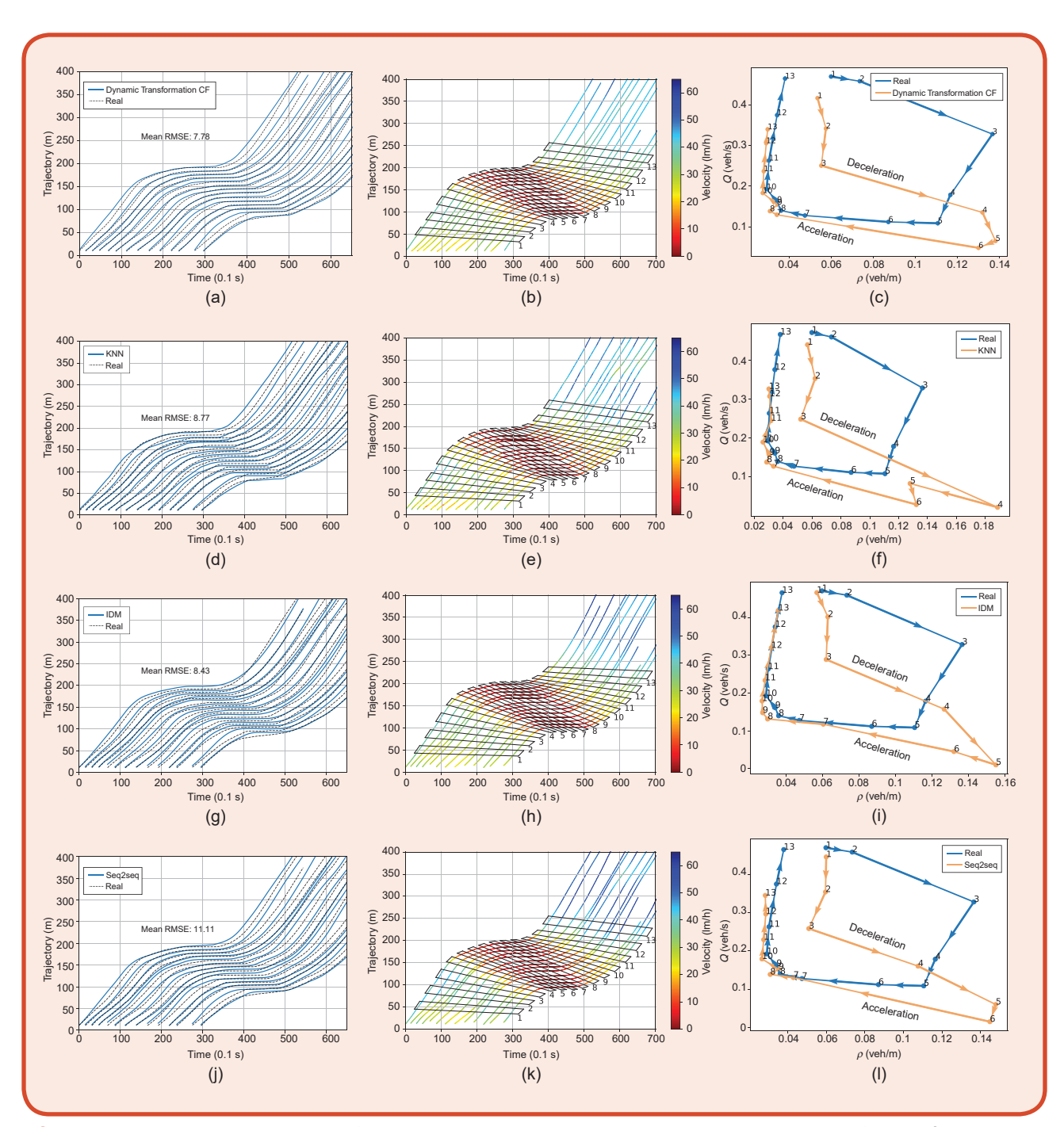


FIG 14 Time-space diagram and hysteresis loop of first vehicle platoon (Lead vehicle 442). (a) Vehicle platoon (Dynamic transformation CF model). (b) Vehicle platoon heatmap (Dynamic transformation CF model). (c) Hysteresis loop (Dynamic transformation CF model). (d) Vehicle platoon (KNN). (e) Vehicle platoon heatmap (KNN). (f) Hysteresis loop (KNN). (g) Vehicle platoon (IDM). (h) Vehicle platoon heatmap (IDM) (i) Hysteresis loop (IDM). (j) Vehicle platoon (Seq2seq). (k) Vehicle platoon heatmap (Seq2seq). (l) Hysteresis loop (Seq2seq).

significantly greater than those of the KNN and dynamic transformation CF model during the 35–60-s time periods. Moreover, although the KNN CF model performed well in trajectory simulation, its space headway error was still greater than that of the dynamic transformation CF model. Figure 13(e) compares the cumulative trajectory RMSE with other models. The cumulative RMSE of the dynamic transformation CF model is approximately 2,000, whereas the range for the other three models is between 4,000 and 5,000, indicating that the dynamic transformation CF model is better able to simulate CF behavior.

Figure 13(f) is provided to further investigate the relationship between the trajectory and cumulative RMSE. The FV deceleration and acceleration phases are where the intervals of a rapid increase in cumulative RMSE are most concentrated. In addition, asymmetric driving behavior (often referred to as a *hysteresis loop*) is a crucial aspect of CF behavior, revealing the asymmetric relationship between space headway and acceleration. Specifically, when the vehicle is in the acceleration state, its space headway is larger, whereas when it is in the deceleration state, its space headway is smaller. Figure 13(g) and (h) demonstrates that the range of velocity and space simulated by the dynamic transformation CF model corresponds to the realistic data.

Mesoscopic Traffic Flow Simulation

The CF behavior is also significant for the mesoscopic traffic flow, i.e., the vehicle platoon. For simulation experiments, the vehicle platoons with the preceding vehicle numbers 442 and 1855 are extracted from the NGSIM dataset; these platoons contain one and multiple stop-and-go waves, respectively. In this section, first, the time-space diagrams of each platoon are presented to compare the performance of the

proposed dynamic transformation CF model and the other three CF models when simulating the traffic oscillation. Second, similar to the asymmetric driving behavior study of the microscopic flow simulation, the method that was proposed by literature [32] is used to plot the hysteresis loop of the vehicle platoon. Third, the boxplot of RMSE for various CF models is provided.

The First Vehicle Platoon (Lead Vehicle 442)

Figure 14 illustrates the trajectory, trajectory heatmap, and hysteresis loop of four CF models. In terms of comparing the FV trajectories, the simulated trajectory by the dynamic transformation CF model is more consistent with the actual data. Moreover, compared to KNN, IDM, and Seq2seq, the dynamic transformation CF model reduces error by 7.71–29.97%. Both indicate that the proposed dynamic transformation CF model has better platoon CF simulation stability.

The boxplot of the trajectory RMSE of the first vehicle platoon is given in Figure 15(a). Figure 15(a) demonstrates that the interquartile range of the dynamic transformation CF model and IDM CF models is less than that of the KNN and Seq2seq CF models. Moreover, although the median of the RMSE of the IDM CF model is lower than that of the dynamic transformation CF model, the IDM has an outlier with a value of 21.20 m. It affected the IDM CF model's stability. In contrast, the dynamic transformation CF model has no outliers, indicating that the dynamic transformation CF model simulates the CF behavior more stable than the IDM CF model.

The Second Vehicle Platoon (Lead Vehicle 1855)

The first vehicle platoon contains only one traffic oscillation segment, while in real traffic scenarios, the vehicle platoon may contain multiple traffic oscillations. The

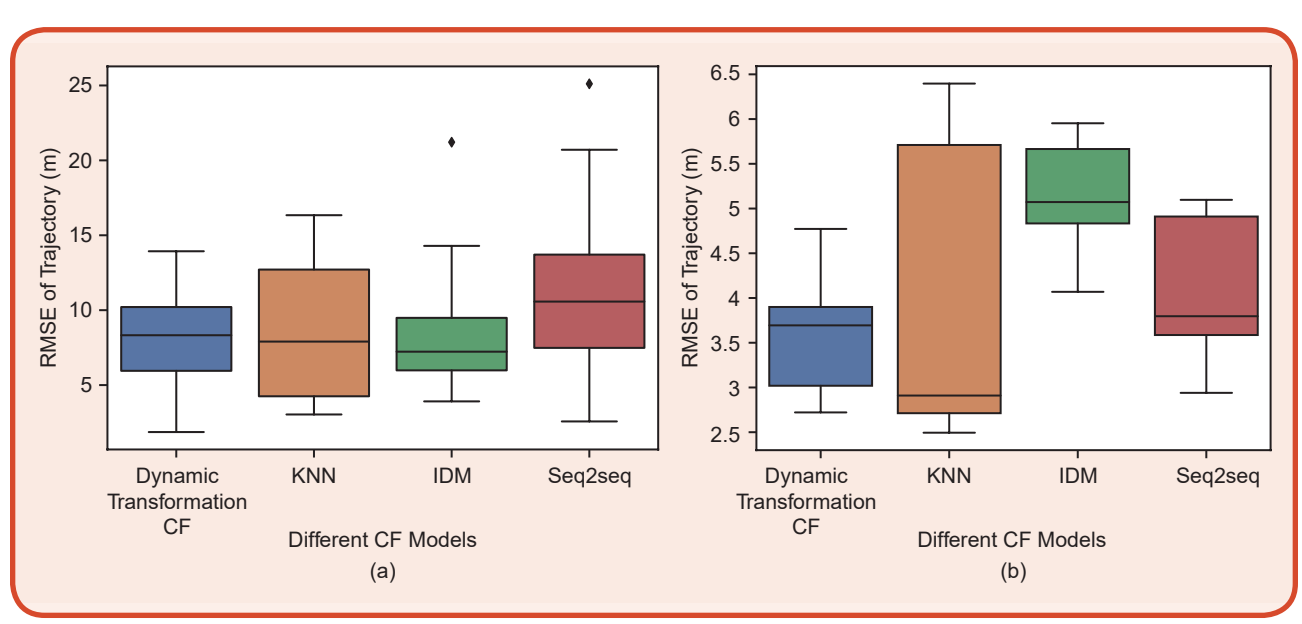


FIG 15 (a) and (b) The boxplot of the trajectory RMSE of two vehicle platoons.

second vehicle platoon (lead vehicle 1855) is therefore extracted from lane 1 in the NGSIM dataset. Figure 16 depicts the time-space diagram and hysteresis loop of the second vehicle platoon. Compared to KNN, IDM, and Seq2seq, the dynamic transformation CF model reduces error by 10.39–29.29%. The dynamic transformation CF

model accurately simulates the trajectory of the fifth FV in Figure 16(a), whereas other models have larger errors. In addition, only the dynamic transformation CF model replicates the two oscillations in the hysteresis loop simulation, and the other three models simulate them poorly in the hysteresis loop simulation.

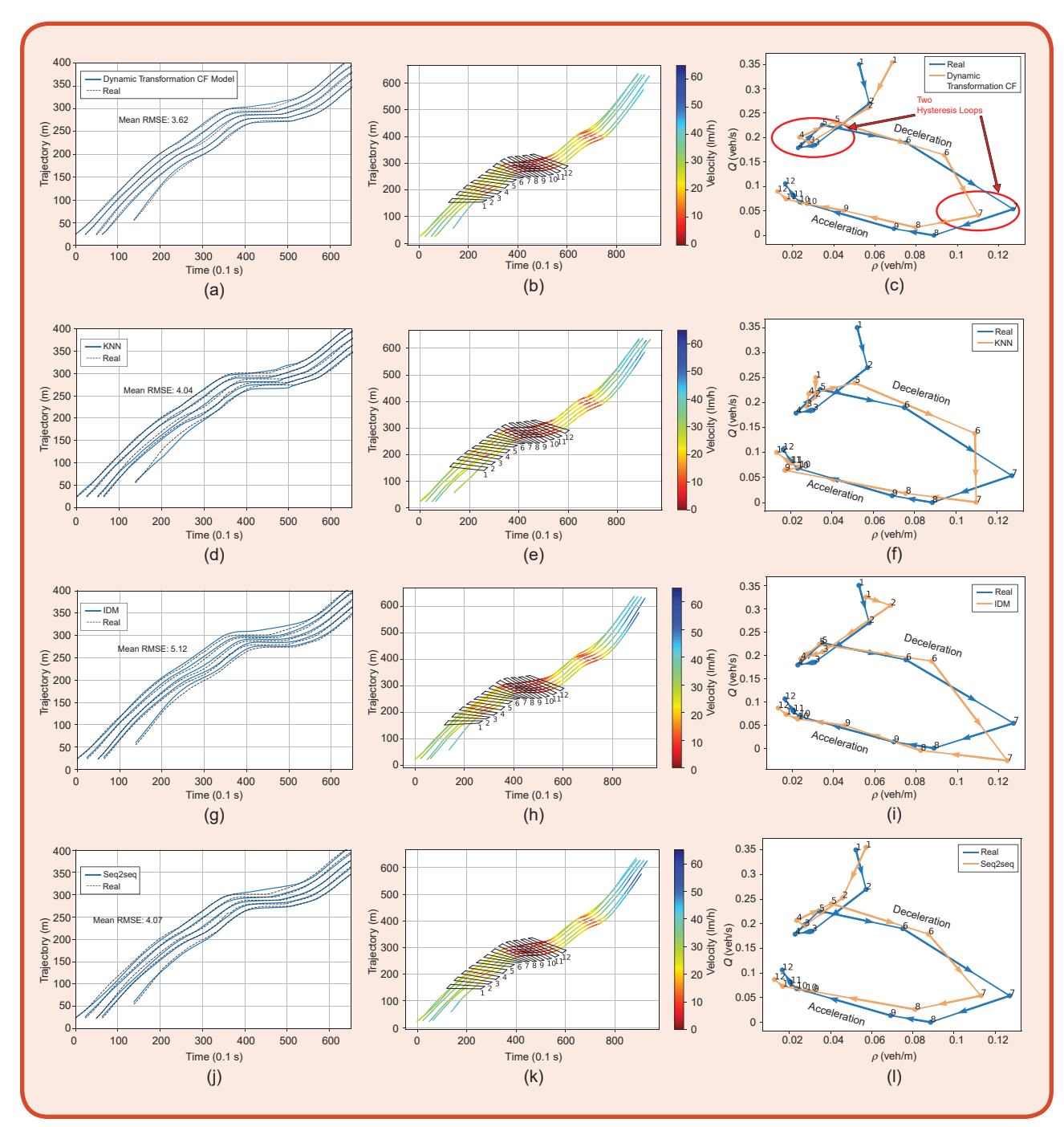


FIG 16 The time-space diagram and hysteresis loop of the second vehicle platoon (lead vehicle 1855). (a) Vehicle platoon (dynamic transformation CF model). (b) Vehicle platoon heatmap (dynamic transformation CF model). (c) Hysteresis loop (dynamic transformation CF model). (d) Vehicle platoon (KNN). (e) Vehicle platoon heatmap (KNN). (f) Hysteresis loop (KNN). (g) Vehicle platoon (IDM). (h) Vehicle platoon heatmap (IDM). (i) Hysteresis loop (IDM). (j) Vehicle platoon (Seq2seq). (k) Vehicle platoon heatmap (Seq2seq). (l) Hysteresis loop (Seq2seq).

Figure 15(b) depicts a boxplot of the second vehicle platoon's trajectory RMSE for each of the four CF models to determine the overall error of the second vehicle platoon. For the second vehicle platoon, the interquartile ranges of the dynamic transformation CF model and IDM CF models were smaller than those of the KNN and Seq2seq models, and the interquartile range of the KNN CF model was the largest of the four CF models, indicating that the RMSE of the trajectory simulated by the KNN CF model for each vehicle is distributed unevenly. Moreover, the minimum and maximum RMSE values of the trajectory simulated by the dynamic transformation CF model are less than those of the other three CF models.

The Virtual Vehicle Platoon Simulation

To further evaluate the performance of the dynamic transformation CF model in simulating a large number of FVs, simulation tests of virtual vehicle platoons were conducted using the following simulation parameters. We assume that the length of the road is 5,000 m, that the initial velocity is 40 km/h, and that 60 vehicles enter the ring road sequentially with a 30-m space headway between each vehicle. Additionally, two traffic disturbances are introduced into the first vehicle. The velocity of the first vehicle will slow down to 0 km/h and idle for 10 s before accelerating when it is under traffic disturbance. Except for the first vehicle, all other vehicles follow the CF strategy planned by the dynamic transformation CF model, and no additional traffic disturbances are introduced. The simulation was implemented, and Figure 17 (a) and (b) depict the time-space diagram and time velocity of the virtual vehicle platoon, respectively. The dynamic transformation CF model is found to accurately represent the entire traffic oscillation propagation process in traffic flow.

Local stability analysis and string analysis are typical methods for evaluating the stability of model-driven CF

models. Due to the absence of a unique mathematical expression for the data-driven CF model, it is impossible to analyze the local stability and string stability of the dynamic transformation CF model with mathematical methods. Nevertheless, the local and string stability of the dynamic transformation CF model could be analyzed according to the definition of local stability and string stability. As depicted in Figure 17(b), the FV's velocity recovers gradually after encountering a traffic disturbance, indicating that the dynamic transformation CF model is locally stable. As depicted in Figure 17(a), the fluctuation amplitude of the FV simulated by the dynamic transformation CF model following a traffic disturbance decreased gradually over time. Taking the first traffic disturbance shown in the black ellipse as an example, the FVs encountered the disturbance at a minimum velocity of 0-10 km/h during the time range of 21–55 s, at a minimum velocity of 10–20 km/h during the time range of 55-75 s and at a minimum velocity of 20–30 km/h during the time range of 75–115 s. The aforementioned experimental results indicate that the dynamic transformation CF model is string stable. On the other hand, as shown in Figure 17(b), during the speed recovery process, the speed of some vehicles may exhibit a sharp deceleration. This indicates that there is room for improvement in our model.

Macroscopic Traffic Flow Simulation

In the virtual simulation of CAV testing, a large number of human-like background vehicles need to be generated to simulate the real traffic flow, and the CF model is a crucial tool for simulating the real traffic flow. To evaluate the accuracy and effectiveness of the dynamic transformation CF model in simulating large-scale traffic flow, all CF pairs of lanes 1 and 4 were extracted from the NGSIM dataset between 7:50 a.m. and 8:05 a.m. Figure 18 (a)-(d)

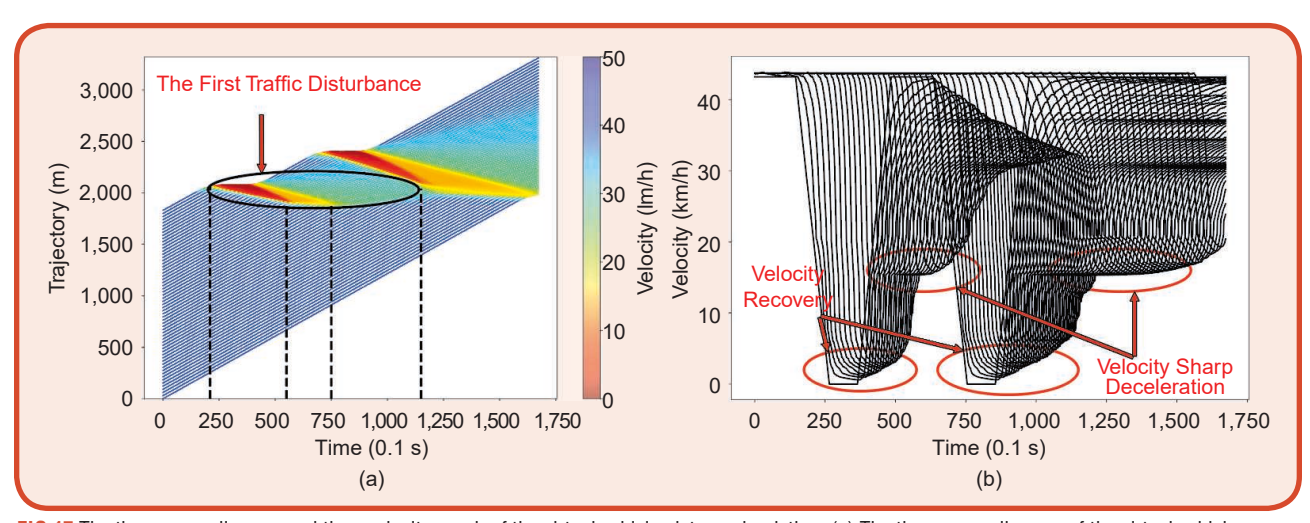


FIG 17 The time-space diagram and time-velocity graph of the virtual vehicle platoon simulation. (a) The time-space diagram of the virtual vehicle platoon. (b) The time-velocity diagram of the virtual vehicle platoon (Acceleration).

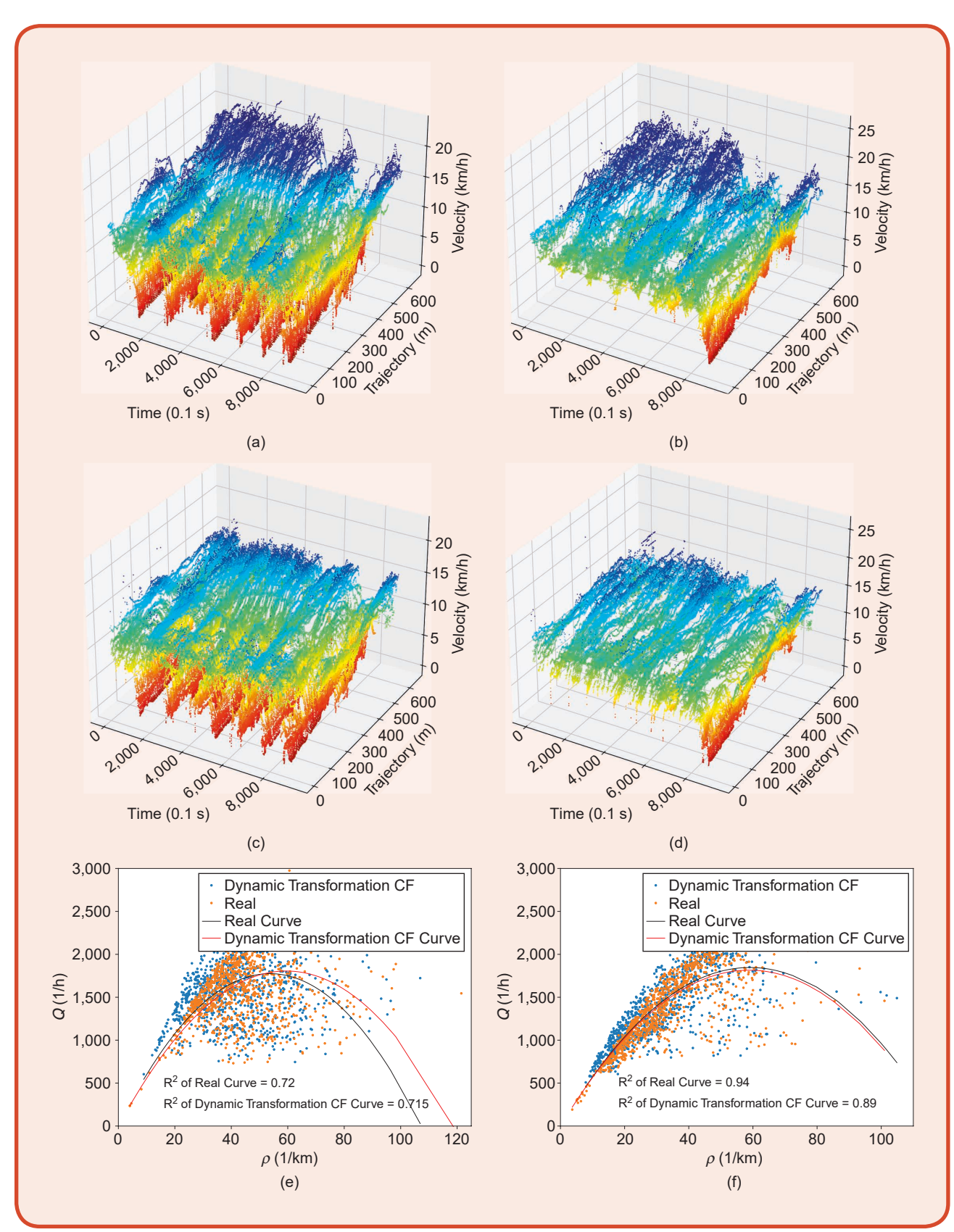


FIG 18 The velocity-time-space diagram and flow-density diagram of real data and dynamic transformation CF model with Lane 1 and Lane 4 data were extracted from the NGSIM dataset.

depicts the results of velocity-time-space diagrams for lanes 1 and 4. It can be seen that the dynamic transformation CF model can replicate many traffic oscillations on lane 1 and few traffic oscillations on lane 4 well. Compared to KNN, IDM, and Seq2seq, the dynamic transformation CF model reduces the lane 1 error by 1.59–11.40%. Compared to KNN, IDM, and Seq2seq, the dynamic transformation CF model reduces the lane 4 error by 4.80–18.26%. The flow-density diagrams of lanes 1 and 4 are shown in Figure 18 (e) and (f) using the Greenshields model. They indicate that the velocity and trajectory simulated by the dynamic transformation CF model of lanes 1 and 4 are approximately the same as the actual velocity and trajectory.

Additionally, the flow, density, and average velocity of the remaining three CF models are calculated. According to Table 7, the RMSE of the three parameters calculated by the

Table 7. The RMSE of flow (vehicles/h), density (vehicles/km), and velocity (km/h) of four CF models. RMSE of Flow, Density, and Velocity of Dynamic Transformation Lane 1 Lane 4 Q V Q V р р 500.54 20.16 17.56 598.7 21.19 16.07 RMSE of Flow, Density, and Velocity of KNN Lane 1 Lane 4 V Q V Q р р 523.48 20.22 18.46 602 21.8 17.25 RMSE of Flow, Density, and Velocity of IDM Lane 1 Lane 4 Q V Q V р р 544.26 20.82 19.64 771.88 24.89 18.08 RMSE of Flow, Density, and Velocity of Seq2seq Lane 1 Lane 4 Q V Q V р р 518.43 20.11 762.98 18.38 20.68 24.86 The bold values are the results obtained by the proposed model.

Table 8. The comparison of different CF models.							
Runtime of Dynamic Runtime of Transformation CF Runtime Runtime Seq2seq Lane ID Model (Inference) of KNN of IDM (Inference)							
Lane 1	115.98	342.3	135.55	81.74			
Lane 4	65.21	221.58	88.37	62.44			

dynamic transformation CF model is smaller than that of the KNN, IDM, and Seq2seq models.

On the other hand, we evaluate the performance of four distinct CF models. In accordance with the definitions of training time and inference time in DL models, the inference times of the dynamic transformation CF model and Seg2seg models are calculated as the runtime when simulating large-scale traffic flow. Table 8 provides a comparison of the runtime results of the four CF models. It demonstrates that the runtime of the dynamic transformation CF model (Inference) was less than the KNN and IDM models but higher than the Seg2seg (Inference) model. The possible reason is that the long-time prediction submodel and Seq2seq output the FV acceleration for multi-time steps simultaneously, whereas the short-time prediction submodel, KNN, and IDM output only the FV acceleration for a single time step at once. The difference between the computational efficiencies of the different CF models is further magnified when simulating the large-scale traffic flow. In addition, if the training time of the DL model is calculated, the dynamic transformation CF model proposed in this article required an additional 258.03 s for training, while the Seq2seq CF model required an additional 44.09 s for training. This is because the dynamic transformation CF model contains the long-time prediction submodel and short-time prediction submodel. Thus, it is more complicated than the Seq2seq CF model.

Conclusion

This article investigates why the IDM CF model cannot accurately simulate the traffic oscillation and demonstrates that data-driven CF models cannot simultaneously account for the inherent correlation between the various vehicle dynamic parameters at the same time step. A dynamic transformation strategy is proposed to divide the traffic oscillation into four phases: coasting, deceleration, acceleration, and stationary. In the proposed framework, a novel dynamic transformation CF model based on the two submodels is proposed to simulate the various phases of the traffic oscillation. The first submodel is based on a modified Seq2seq and takes into account the inherent correlation between the various vehicle dynamic parameters at the same time step. The second submodel, which is based on the Transformer model, captures acceleration changes during acceleration and deceleration phases more accurately than other data-driven CF models.

To validate the proposed dynamic transformation CF model, a DL- and traffic flow-based evaluation framework comprising various traffic parameters is developed. In the DL simulation test, the ability of various data-driven CF models to capture long-time sequence data is compared, with the results indicating that the proposed model performed better. In addition, the dynamic transformation CF

model is compared to three representative models (KNN, IDM, and Seq2seq) from micro, meso, and macro perspectives. In the microscopic simulation, the acceleration, velocity, trajectory, and space headway of various CF models are evaluated. In the mesoscopic simulation, a comparison is made in the trajectory generation of the vehicle platoon and hysteresis loop. Furthermore, the virtual vehicle platoon generation simulation is conducted to validate the local and string stability of the dynamic transformation CF model. In the macroscopic simulation, all CF pairs are simulated for 15 minutes on a single road by four CF models; the trajectory, flow, and density are used to test the different CF models. In addition, the runtime of various CF models is compared. The experimental results demonstrate that not only is the proposed dynamic transformation CF model more accurate than the other three CF models, but its simulation efficiency is also superior.

It is necessary to further combine other traffic dynamics parameters to divide the four phases of the traffic oscillation more accurately and dynamically so that it can be utilized more effectively for the simulation of realistic CF behavior and the generation of large-scale traffic flow. The framework proposed in this article is an important foundation for future research.

Acknowledgment

This work was supported by the National Key Research and Development Program of China (Grant 2021YFB2501200), the National Natural Science Foundation of China (Grant 61703053), the Shaanxi Province Key Research and Development Program (Grant 2022GY-300), the Chang'an University Graduate Student Innovation Ability Cultivation Project (Grant 300203211242), and the Key Project of National Natural Science Foundation of China (Grant 52220105001) and sponsored by the Tsinghua-Toyota Joint Research Fund.

About the Authors



Shan Fang (fang6100146@gmail.com) earned his B.S. degree in computer science from Jilin University, Changchun, China, in 2016. He is currently pursuing his Ph.D. degree at the School of Information Engineering, Chang'an University, Xi'an 710064, China. His re-

search interests include traffic flow simulation and cooperative eco-driving strategies for vehicles.



Lan Yang (lanyang@chd.edu.cn) earned her Ph.D. degree in traffic information engineering and control from Chang'an University, Xi'an, China, in 2013. She is currently a professor at the School of Information Engineering, Chang'an University, Xi'an 710064, China. She was with the University of California, Riverside as a visiting scholar in 2020. Her research interests include connected and autonomous vehicles, traffic flow analysis, eco-driving, and intelligent transportation systems.



Xiangmo Zhao (xmzhao@chd.end.cn) earned his Ph.D. degree from Chang'an University, Xi'an, China, in 2006. He is currently a professor at the School of Information Engineering, Chang'an University, Xi'an 710064, China. He is the vice-president of the Joint Laboratory for

Connected Vehicles, the Ministry of Education and China Mobile, and the Shaanxi Road Traffic Intelligent Detection and Equipment Engineering Technology Research Centre and a leader of the National Key Subjects-Traffic Information Engineering and Control, Chang'an University. His research interests include connected vehicles, automated vehicles, intelligent transportation systems, and computer science. He is the director of the Information Professional Committee; a member of the Advisory Expert Group of the China Transportation Association, the National Motor Vehicle Operation Safety Testing Equipment Standardization Committee, and the Leading Group of the National Traffic Computer Application Network; the vice-chairman of the Institute of Highway Association on Computer Professional Committee; and the deputy director of the Institute of Computer in Shaanxi Province.



Wei Wang (wei.wang@chd.edu.cn) earned his Ph.D. degree in electronics and information engineering from the University of Erlangen-Nuremberg, Erlangen, Germany, in 2014. From 2007 to 2017, he was a scientific researcher with the German

Aerospace Center (DLR). He is currently a professor at the School of Information Engineering, Chang'an University, Xi'an 710064, China. His research interests include wireless channels and positioning and navigation technology.



Zhigang Xu (xuzhigang@chd.edu.cn) earned his Ph.D. degree in traffic information engineering and control from Chang'an University, Xi'an, China, in 2012. He is currently a professor at the School of Information Engineering, Chang'an University, Xi'an 710064,

China, and the director of the Lab of Traffic information Sensing and Control at Chang'an University. He was with the University of California, Davis as a visiting scholar in 2015. His research interests include connected and autonomous vehicles, traffic flow analysis, transportation optimization, and intelligent transportation systems. He is the chair of the CAVs Committee of the World Transportation Convention and a member of the IEEE Intelligent Transportation Systems Society and the American Society of Civil Engineers.



Guoyuan Wu (guoyuan.wu@ucr.edu) earned his Ph.D. degree in mechanical engineering from the University of California, Berkeley in 2010. Currently, he holds an associate research engineer position in the Transportation Systems Research Group at the Bourns

College of Engineering Center for Environmental Research and Technology and an associate adjunct professor position in electrical and computer engineering at the University of California at Riverside, Riverside, CA 92521-9800 USA. His research interests include the development and evaluation of sustainable and intelligent transportation systems technologies, including connected and automated transportation systems, optimization and control of vehicles, and traffic modeling and simulation. He is an associate editor of the SAE Journal of Connected and Automated Vehicles and a member of the Vehicle-Highway Automation Committee (AHB30) of the Transportation Research Board. He is also a board member of the Chinese Institute of Engineers Southern California Chapter (CIE-SOCAL) and a member of the Chinese Overseas Transportation Association.



Yang Liu (liuy@chalmers.se) is a Marie Curie Fellow at the Department of Architecture and Civil Engineering, Chalmers University of Technology, 412 96 Gothenburg, Sweden. He serves as a Young Editor for two top-tier academic journals, including *The Innova-*

tion and IEEE/CAA Journal of Automatica Sinica. In addition, he is an associate editor of the Journal of Intelligent and Connected Vehicles. He leads a European Union project and a project funded by the Swedish Innovation Agency. His work has been published in top international journals in the fields of intelligent transportation and automation, such as IEEE Transactions on Cybernetics, IEEE Transactions on Intelligent Transportation Systems, IEEE/ CAA Journal of Automatica Sinica, IEEE Intelligent Transportation Systems Magazine, and CACAIE Transportation Research Part A/C/E. He has received numerous awards for his research, including the IEEE ITSM Best Paper High Commendation Award, Honorable Mention of the COTA Best Dissertation Award, the ICME Grand Challenge Second Runner-up Award, and the China Highway Society Outstanding Doctoral Dissertation Award. He is experienced in the practice of artificial intelligence (AI) techniques and has won several world prizes in AI competitions

organized by leading international AI conferences or research institutes (e.g., KDD, IJCAI, NeurIPS, CVPR, ICME, and TRB), including first place in the KDD Cup, the most well-known algorithm competition in data mining. He is a Member of IEEE.



Xiaobo Qu (xiaobo@tsinghua.edu.cn) is a chair professor at the State Key Laboratory of Automotive Safety and Energy, School of Vehicle and Mobility, Tsinghua University, Beijing 100084, China. His research interests include enhancing urban mobility systems

by incorporating emerging technologies, particularly for emergency services and connected automated vehicles. He has authored or coauthored more than 120 journal articles published in top-tier journals, including 14 Essential Science Indicators highly cited articles. He serves as an editor for 10 journals, including the editor-in-chief of Communications in Transportation Research and executive editorin-chief of the Journal of Intelligent and Connected Vehicles. To date, he has secured research funding well above €10 million from the Australian Research Council, Swedish Innovation Agency Vinnova, STINT, and the European Union. He has been invited to serve as a panel/assessor for prestigious funding schemes such as the Australian Research Council Centre of Excellence (AUD\$35 million each), Future Fellowship (career grant, AUD\$1 million each), Netherlands NWO VICI (career grant, €2.5 million each), Hong Kong Research Council theme based scheme (HKD\$30 million each), Singapore Ministry of Education Thematic Research Program (SD\$5 million each), and the European Research Council, etc. He has also been an elected member of Academia Europaea (the Academy of Europe) since August 2020 and a fellow of the Institution of Engineering and Technology.

References

- X. Zhu et al., "Interaction-aware cut-in trajectory prediction and risk assessment in mixed traffic," *IEEE/CAA J. Automatica Sinica*, vol. 9, no. 10, pp. 1752–1762, Oct. 2022, doi: 10.1109/JAS.2022.105866.
- [2] T. Feng, L. Liu, X. Xing, and J. Chen, "Multimodal critical-scenarios search method for test of Autonomous Vehicles," J. Intell. Connected Vehicles, vol. 5, no. 3, pp. 167–176, 2022, doi: 10.1108/JICV-04-2022-0016.
- [5] Z. Xu, Y. Fang, N. Zheng, and H. L. Vu, "Analyzing the inconsistency in driving patterns between manual and autonomous modes under complex driving scenarios with a VR-enabled simulation platform," *J. Intell. Connected Vehicles*, vol. 5, no. 3, pp. 215–234, Dec. 2022, doi: 10.1108/JICV-05-2022-0017.
- [4] N. Lyu, Y. Wang, C. Wu, L. Peng, and A. F. Thomas, "Using naturalistic driving data to identify driving style based on longitudinal driving operation conditions," *J. Intell. Connected Vehicles*, vol. 5, no. 1, pp. 17–35, 2022, doi: 10.1108/JICV-07-2021-0008.
- [5] S. Acharya and M. Mekker, "Importance of the reputation of data manager in the acceptance of connected vehicles," *Commun. Transp. Res.*, vol. 2, Dec. 2022, Art. no. 100053, doi: 10.1016/j.commtr.2022.100053.
- [6] T. Olovsson, T. Svensson, and J. Wu, "Future connected vehicles: Communications demands, privacy and cyber-security," Commun. Transp. Res., vol. 2, Dec. 2022, Art. no. 100056, doi: 10.1016/j.commtr.2022.100056.
- [7] Y. Liu, R. Jia, J. Ye, and X. Qu, "How machine learning informs ridehailing services: A survey," *Commun. Transp. Res.*, vol. 2, Dec. 2022, Art. no. 100075, doi: 10.1016/j.commtr.2022.100075.

- [8] Y. Liu, F. Wu, C. Lyu, S. Li, J. Ye, and X. Qu, "Deep dispatching: A deep reinforcement learning approach for vehicle dispatching on online ride-hailing platform," *Transp. Res. E, Logistics Transp. Rev.*, vol. 161, May 2022, Art. no. 102694, doi: 10.1016/j.tre.2022.102694.
 [9] J. Xu, Y. Zhang, Z. Dai, F. Li, and J. Chen, "Vehicle trajectory oscilla-
- [9] J. Xu, Y. Zhang, Z. Dai, F. Li, and J. Chen, "Vehicle trajectory oscillation characteristics and lane width control under human natural driving conditions," J. Automot. Saf. Energy, vol. 13, no. 4, pp. 718–728, 2022.
- [10] M. Hu et al., "Hierarchical cooperative control of connected vehicles: From heterogeneous parameters to heterogeneous structures," *IEEE/CAA J. Automatica Sinica*, vol. 9, no. 9, pp. 1590–1602, Sep. 2022, doi: 10.1109/JAS.2022.105556.
- [11] Y. Liu, F. Wu, Z. Liu, K. Wang, F. Wang, and X. Qu, "Can language models be used for real-world urban-delivery route optimization?" *Innovation*, early access, Sep. 2023, doi: 10.1016/j.xinn.2023.100520.
- [12] Y. Zheng et al., "Lateral velocity estimation for four-wheel-independent-drive electric vehicles based on deep reinforcement learning," J. Automot. Saf. Energy, vol. 15, no. 1, pp. 131–141, 2022.
- [13] B. Liu et al., "Microscopic trajectory data-driven probability distribution model for weaving area of channel change," *J. Automot. Saf. Energy*, vol. 15, no. 2, pp. 550–540, 2022.
 [14] T. Ruan, H. Wang, L. Zhou, Y. Zhang, C. Dong, and Z. Zuo, "Impacts
- [14] T. Ruan, H. Wang, L. Zhou, Y. Zhang, C. Dong, and Z. Zuo, "Impacts of information flow topology on traffic dynamics of CAV-MV heterogeneous flow," *IEEE Trans. Intell. Transp. Syst.*, vol. 23, no. 11, pp. 20,820–20,835, Nov. 2022, doi: 10.1109/TITS.2022.3170965.
- [15] T. Luong, H. Pham, and C. D. Manning, "Effective approaches to attention-based neural machine translation," in *Proc. Conf. Empirical Methods Natural Lang. Process.*, 2015, pp. 1412–1421, doi: 10.18653/v1/D15-1166.
- [16] H. Xing and Y. Liu, "Graph attention network for car-following model under game between desired and real state," *IET Intell. Transport* Syst., vol. 16, no. 6, pp. 800–812, Jun. 2022, doi: 10.1049/itr2.12175.
- [17] Z. Mo, R. Shi, and X. Di, "A physics-informed deep learning paradigm for car-following models," *Transp. Res. C, Emerg. Technologies*, vol. 130, Sep. 2021, Art. no. 103240, doi: 10.1016/j.trc.2021.103240.
 [18] M. Zhou, X. Qu, and X. Li, "A recurrent neural network based micro-
- [18] M. Zhou, X. Qu, and X. Li, "A recurrent neural network based microscopic car following model to predict traffic oscillation," *Transp. Res. C, Emerg. Technologies*, vol. 84, pp. 245–264, Nov. 2017, doi: 10.1016/j. trc.2017.08.027.
- [19] L. Ma and S. Qu, "A sequence to sequence learning based car-following model for multi-step predictions considering reaction delay," *Transp. Res. C, Emerg. Technologies*, vol. 120, Nov. 2020, Art. no. 102785, doi: 10.1016/j.trc.2020.102785.
- [20] Y. Yu, Z. He, and X. Qu, "On the impact of prior experiences in car-following models: Model development, computational efficiency, comparative analyses, and extensive applications," *IEEE Trans. Cybern.*, vol. 53, no. 3, pp. 1405–1418, Mar. 2023, doi: 10.1109/TCYB.2021.3095154.
- [21] A. Vaswani et al., "Attention is all you need," in Proc. Adv. Neural Inf. Process. Syst., 2017, pp. 5998–6008.
- [22] Y. Yu, R. Jiang, and X. Qu, "A modified full velocity difference model with acceleration and deceleration confinement: Calibrations, validations, and scenario analyses," *IEEE Intell. Transp. Syst. Mag.*, vol. 15, no. 2, pp. 222–235, Summer 2021, doi: 10.1109/MITS.2019.2898965.
- [23] M. Treiber, A. Hennecke, and D. Helbing, "Congested traffic states in empirical observations and microscopic simulations," *Physical Rev. E*, vol. 62, no. 2, pp. 1805–1824, Aug. 2000, doi: 10.1103/PhysRevE.62.1805.
- [24] G. F. Newell, "A simplified car-following theory: A lower order model," Transp. Res. B, Methodological, vol. 36, no. 3, pp. 195–205, Mar. 2002, doi: 10.1016/S0191-2615(00)00044-8.
- [25] X. Li, X. Wang, and Y. Ouyang, "Prediction and field validation of traffic oscillation propagation under nonlinear car-following laws," *Transp. Res. B, Methodological*, vol. 46, no. 3, pp. 409–423, Mar. 2012, doi: 10.1016/j.trb.2011.11.003.
- [26] X. Li, J. Cui, S. An, and M. Parsafard, "Stop-and-go traffic analysis: Theoretical properties, environmental impacts and oscillation mitigation," *Transp. Res. B, Methodological*, vol. 70, pp. 519–539, Dec. 2014, doi: 10.1016/j.trb.2014.09.014.
- [27] C. Rhoades, X. Wang, and Y. Ouyang, "Calibration of nonlinear carfollowing laws for traffic oscillation prediction," *Transp. Res. C, Emerg. Technologies*, vol. 69, pp. 328–342, Aug. 2016, doi: 10.1016/j. trc.2016.05.018.
- [28] J. Sun, Z. Zheng, and J. Sun, "The relationship between car following string instability and traffic oscillations in finite-sized platoons and its use in easing congestion via connected and automated vehicles with IDM based controller," Transp. Res. B, Methodological, vol. 142, pp. 58–83, Dec. 2020, doi: 10.1016/j.trb.2020.10.004.
- [29] V. Papathanasopoulou and C. Antoniou, "Towards data-driven carfollowing models," *Transp. Res. C, Emerg. Technologies*, vol. 55, pp. 496–509, Jun. 2015, doi: 10.1016/j.trc.2015.02.016.
- [50] Z. He, L. Zheng, and W. Guan, "A simple nonparametric car-following model driven by field data," *Transp. Res. B, Methodological*, vol. 80, pp. 185–201, Oct. 2015, doi: 10.1016/j.trb.2015.07.010.

- [51] D. Yang, L. Zhu, Y. Liu, D. Wu, and B. Ran, "A novel car-following control model combining machine learning and kinematics models for automated vehicles," *IEEE Trans. Intell. Transp. Syst.*, vol. 20, no. 6, pp. 1991–2000, Jun. 2019, doi: 10.1109/TITS.2018.2854827.
- [52] L. Li, R. Jiang, Z. He, X. Chen, and X. Zhou, "Trajectory data-based traffic flow studies: A revisit," *Transp. Res. C, Emerg. Technologies*, vol. 114, pp. 225–240, May 2020, doi: 10.1016/j.trc.2020.02.016.
- [33] M. Zhu, X. Wang, and Y. Wang, "Human-like autonomous car-following model with deep reinforcement learning," Transp. Res. C, Emerg. Technologies, vol. 97, pp. 348–368, Dec. 2018, doi: 10.1016/j.trc.2018.10.024.
- [54] M. Zhu, Y. Wang, Z. Pu, J. Hu, X. Wang, and R. Ke, "Safe, efficient, and comfortable velocity control based on reinforcement learning for autonomous driving," *Transp. Res. C, Emerg. Technologies*, vol. 117, Aug. 2020, Art. no. 102662, doi: 10.1016/j.trc.2020.102662.
- [35] M. Zhou, Y. Yu, and X. Qu, "Development of an efficient driving strategy for connected and automated vehicles at signalized intersections: A reinforcement learning approach," *IEEE Trans. Intell. Transp. Syst.*, vol. 21, no. 1, pp. 433–443, Jan. 2020, doi: 10.1109/TITS.2019.2942014.
- [56] X. Qu, Y. Yu, M. Zhou, C.-T. Lin, and X. Wang, "Jointly dampening traffic oscillations and improving energy consumption with electric, connected and automated vehicles: A reinforcement learning based approach," Appl. Energy, vol. 257, Jan. 2020, Art. no. 114030, doi: 10.1016/j.apenergy.2019.114050.
- [37] D. Song, B. Zhu, J. Zhao, J. Han, and Z. Chen, "Personalized car-following control based on a hybrid of reinforcement learning and supervised learning," *IEEE Trans. Intell. Transp. Syst.*, vol. 24, no. 6, pp. 6014–6029, Jun. 2023, doi: 10.1109/TITS.2023.3245362.
- [38] H. Jia, Z. Juan, and A. Ni, "Develop a car-following model using data collected by 'five-wheel system'," in Proc. IEEE Int. Conf. Intell. Transp. Syst., Oct. 2003, vol. 1, pp. 346–351, doi: 10.1109/ITSC.2003.1251975.
- [59] S. Panwai and H. Dia, "Neural agent car-following models," *IEEE Trans. Intell. Transp. Syst.*, vol. 8, no. 1, pp. 60-70, Mar. 2007, doi: 10.1109/TITS.2006.884616.
- [40] A. Khodayari, A. Ghaffari, R. Kazemi, and R. Braunstingl, "A modified car-following model based on a neural network model of the human driver effects," *IEEE Trans. Syst.*, Man, Cybern. Syst., vol. 42, no. 6, pp. 1440–1449, Nov. 2012, doi: 10.1109/TSMCA.2012.2192262.
- [41] J. Zheng, K. Suzuki, and M. Fujita, "Car-following behavior with instantaneous driver-vehicle reaction delay: A neural-network-based methodology," *Transp. Res. C, Emerg. Technologies*, vol. 36, pp. 339– 351, Nov. 2015, doi: 10.1016/j.trc.2015.09.010.
- [42] C. Colombaroni and G. Fusco, "Artificial neural network models for car following: Experimental analysis and calibration issues," J. Intell. Transp. Syst., vol. 18, no. 1, pp. 5–16, 2014, doi: 10.1080/15472450.2013.801717.
- [45] X. Wang, R. Jiang, L. Li, Y. Lin, X. Zheng, and F.-Y. Wang, "Capturing carfollowing behaviors by deep learning," *IEEE Trans. Intell. Transp. Syst.*, vol. 19, no. 3, pp. 910–920, Mar. 2018, doi: 10.1109/TITS.2017.2706963.
- [44] X. Huang, J. Sun, and J. Sun, "A car-following model considering asymmetric driving behavior based on long short-term memory neural networks," *Transp. Res. C, Emerg. Technologies*, vol. 95, pp. 346–362, Oct. 2018, doi: 10.1016/j.trc.2018.07.022.
- [45] Y. Lin, P. Wang, Y. Zhou, F. Ding, C. Wang, and H. Tan, "Platoon trajectories generation: A unidirectional interconnected LSTM-based car-following model," *IEEE Trans. Intell. Transp. Syst.*, vol. 23, no. 3, pp. 2071–2081, Mar. 2022, doi: 10.1109/TITS.2020.3031282.
- [46] M. Zhu, S. S. Du, X. Wang, Z. Pu, and Y. Wang, "Transfollower: Long-sequence car-following trajectory prediction through transformer," 2022, arXiv:2202.03183.
- [47] D. Xu, G. Gao, Q. Qiu, X. Shang, and H. Li, "A car-following model considering missing data based on TransGAN networks," *IEEE Trans. Intell. Veh.*, early access, 2023, doi: 10.1109/TIV.2023.3270336.
- [48] Y. Zhou et al., "Data-driven analysis for disturbance amplification in car-following behavior of automated vehicles," *Transp. Res. B, Methodological*, vol. 174, Aug. 2023, Art. no. 102768, doi: 10.1016/j. trb.2023.05.005.
- [49] D. Chen, J. A. Laval, S. Ahn, and Z. Zheng, "Microscopic traffic hysteresis in traffic oscillations: A behavioral perspective," *Transp. Res. B, Methodological*, vol. 46, no. 10, pp. 1440–1453, Dec. 2012, doi: 10.1016/j.trb.2012.07.002.
- [50] M. Treiber and A. Kesting, Traffic Flow Dynamics: Data, Models and Simulation. Berlin, Germany: Springer-Verlag, 2013.
- [51] H. Yeo and A. Skabardonis, "Understanding stop-and-go traffic in view of asymmetric traffic theory," in *Transportation and Traffic Theory 2009:* Golden Jubilee. Boston, MA, USA: Springer-Verlag, 2009, pp. 99–115.
- [52] L. Yang et al., "Physical model versus artificial neural network (ANN) model: A comparative study on modeling car-following behavior at signalized intersections," J. Adv. Transp., vol. 2022, pp. 1–18, Apr. 2022, doi: 10.1155/2022/8482846.